OPTIMIZATION OF TWISTED RUDDER (With Bulb and Hub Cap)

Sara Echeverry Jaramillo

Master Thesis

presented in partial fulfillment
of the requirements for the double degree:
"Advanced Master in Naval Architecture" conferred by University of Liege
"Master of Sciences in Applied Mechanics, specialization in Hydrodynamics, Energetic and Propulsion" conferred by Ecole Centrale de Nantes

developed at University of Rostock, Germany
in the framework of the

"EMSHIP"

Erasmus Mundus Master Course in "Integrated Advanced Ship Design"

Ref. 159652-1-2009-1-BE-ERA MUNDUS-EMMC

Supervisor: Prof. Nikolai Kornev, University of Rostock
Reviewer: Prof. Pierre Ferrant, Ecole Centrale de Nantes

Rostock, February 2016

Abstract

This thesis has been carried out in close cooperation with the Fluid Engineering department of the DNV GL SE Maritime Advisory division in Hamburg.

The main role of the Rudder consists not only on acting as a steering device and keep the ship on course, but also is a very significant energy recovery device when interacting with the wake from the propeller. Several studies have been performed in order to analyse the interaction effects between hull, rudder and propeller, assessing drag and manoeuvring characteristics from several geometries looking upon maximising the propulsive efficiency. Twisted rudders in combination with rudder bulbs can improve propulsion efficiency even by up to 4%.

This master thesis consists in the implementation of a rudder optimization procedure with respect to overall propulsion efficiency. More concretely a twisted rudder with costa bulb (and hub cap) evaluated utilizing a CFD process developed in the DNV GL SE facilities, coupling Reynolds-Averaged Navier-Stokes *RANS* method and Boundary Element method *BEM*. Solvers are the stationary *OpenFOAM RANS simpleFoam* and the unsteady *BEM PROCAL*. The use of this coupled method will reduce the computational time requirements compared to a fully *RANS* simulation. Thus the possibility of using an optimization routine (FS-Optmizer) to analyse different geometries for the Twisted Rudder, changing parameters in the CAD model created with CAESES Framework.

The geometry is the *Duisburg Test Case* (DTC) which is a hull design of a typical 14000 TEU container ship in order to compare results to a real test case. A twisted rudder equipped with a Costa bulb is used, with a base symmetric profile (*NACA 0020*); the twist goes from the top and bottom upon the bulb with a maximum angle of 15° along an axis located between 20% and 40% of the chord length.

This document presents a flow work starting with the basic theoretical background, then a detailed description of the method, creation of the parametric model, mesh study followed by an initial non-twisted geometry assessment and in the end the optimization procedure description (for rudder and bulb), presenting final results, conclusions and recommendations.

Keywords: Twisted rudder, optimization, Pareto front, coupled RANS-BEM method

Resumen

Esta tesis de maestría se ha desarrollado en cooperación con el departamento de ingeniería de fluidos de la compañía DNV GL SE en Hamburgo.

La función principal del timón no consiste únicamente en actuar como un elemento de gobierno para mantener el buque en curso sino que también juega un papel importante como elemento recuperador de energía al interactuar con el flujo proveniente de la hélice. Se han realizado algunos estudios sobre la interacción entre casco, hélice y timón con el fin de analizar el arrastre y la maniobrabilidad en diferentes geometrías para asímismo mejorar la eficiencia propulsiva. Los timones torsionados en combinación con bulbos tipo costa pueden mejorar la eficiencia propulsiva en hasta 4 %.

Esta tesis consiste en la implementación de un proceso de optimización a un timón de dirección con respecto a la eficiencia propulsiva, en concreto un timón torsionado junto con un bulbo tipo costa a través de un análisis computacional en esquema acoplado, también desarrollado en las dependecias de DNV GL SE, que consiste en combinar un método *RANSE* con un método de elementos de frontera (*BEM*). Los recursos a utilizar son *OpenFOAM* en estado estacionario a través del solver *simpleFoam* y *PROCAL* con su solver en estado no estacionario. El uso del método acoplado reduce los requerimientos de tiempo computacional comparado con una simulación de tipo *RANSE*, por lo tanto existe la posibilidad de utilizar una rutina de optimización (*FS-Optimizer*) con el fin de analizar diferentes geometrías para el timón mediante la variación de algunos parámetros en el modelo computacional creado con CAESES. La geometría consiste en un *Duisburg Test Case* (DTC), que contiene la carena típica de un portacontenedores de 14000 TEU. Un timón torsoniado y su bulbo son usados, el perfil base es simétrico (*NACA 0020*), la torsión es generada desde los extremos hacia el bulbo con un ángulo máximo de 15° a lo largo de un eje ubicado entre el 20 % y 40 % de la cuerda.

Este documento presenta un flujo de trabajo comenzando con el antecedente teórico, luego una descripción detallada del método, seguidos por la creación del modelo paramátrico, el estudio de malla y análisis de la primera geometría (sin twist) y finalmente la descripción del procedimiento de optimización (para el rudder y bulbo), presentando los resultados finales, como también conclusiones y recomendaciones.

Palabras clave: timón torsionado, optimización, frontera Pareto, método acoplado RANS-BEM

Acknowledgements

This thesis has been carried out between July and December 2015 in cooperation with the Fluid Engineering department of the DNV GL SE Maritime Advisory division in Hamburg. All *Star-CCM+* meshing have been carried out with an educational license kindly provided by CD-adapco. The geometry generation was possible thanks to the kind help of FRIENDSHIP SYSTEMS AG supporting me with the necessary licenses for the *CAESES* framework.

I want to sincerely express my gratitude to my supervisor Dipl.-Ing. Daniel Schmode for his support and guidance through the development of this project. He was always enthusiastic about my work and he trusted me in every step of the research, which always encouraged and motivated me to push myself further.

On the other hand i would like to express my gratitude to the EMSHIP professors for giving me the opportunity to enrol this interesting program, especially to my supervisor in University of Rostock Prof. Nikolai Kornev for his support during the development of this thesis.

Furthermore, my sincere appreciation is extended to the whole Fluid Engineering and Fluid Dynamics departments at the DNV GL office in Hamburg, for providing me with all the assistance and information I could ask for.

Special thanks go to Juryk Henrichs and Frank Lumpitzsch for sharing their experience with the FS-Optimizer. To Uwe Hollenbach for his advices on rudder properties. To Julian Herbel for his patience and continuous help with programming the simulations and new scripts needed. To Sören Schenke for implementing the coupled scheme and teaching me all the steps to use it properly. And to Jan Wieczorek for guiding me with the use of different software running in *Ubuntu*.

I would also thank Álvaro Benet for being with me through all the master giving me continuous moral support and for the proofreading of my thesis. Finally, I would like to express my love and appreciation to my family, who have always been there in the distance. Without them i would have not reached my goals.

This thesis was developed in the frame of the European Master Course in “Integrated Advanced Ship Design” named “EMSHIP” for “European Education in Advanced Ship Design”, Ref.: 159652-1-2009-1-BE-ERA MUNDUS-EMMC.

Contents

List of Figures

List of Tables

List of Abbreviations

BEM	Boundary Element method
CAD	Computer aided design
CFD	Computational Fluid Dynamics
DOE	Design of Experiments
EEDI	Energy Efficiency Design Index
EID	Efficiency Improving Devices
ICCT	International Council on Clean Transportation
IMO	International Maritime Organization
LE	Leading edge
MEPC	Maritime Environment Protection Committee
NACA	National Advisory Committee for Aeronautics
RANS	Reynolds Averaged Navier-Stokes
SVA	Potsdam Model Basin - *Schiffbau-Versuchsanstalt Potsdam*
TE	Trailing edge
TEU	Twenty-foot Equivalent Unit: standard unit to count containers on board of a ship

List of Symbols

Symbol	Unit	Explanation
α	deg	Rudder incidence (twist angle)
A_e/A_0	$-$	Area ratio
AR	$-$	Rudder Aspect ratio
β	deg	Yaw angle between the rudder-propeller combination and free stream
ang_1	deg	Twist angle at rudder top side
ang_2	deg	Twist angle at rudder bottom side
B	m	Beam
c	m	Rudder mean chord
$c_{0.7}$	m	Chord length at $r/R_p = 0.7$
C_B	$-$	Block coefficient
C_{Pc}	m	Center of pressure % of chord from LE
C_{Ps}	m	Center of pressure % of span from root
C_L	$-$	Lift coefficient
C_D	$-$	Drag coefficient
C_F	$-$	Friction resistance coefficient
C_R	$-$	Residual resistance coefficient
C_N	$-$	Normal force coefficient
C_T	$-$	Total resistance coefficient
d	N	Drag force
D_p	m	Propeller diameter
FD	$[N]$	Friction deduction
F_R	$[-]$	Froude Number
Fy_{rudder}	N	Rudder normal force
J	$-$	Advance ratio
K_T	$-$	Propeller thrust coefficient
K_Q	$-$	Propeller torque coefficient
λ	$-$	Scale factor or relaxation factor
L_{pp}	m	Length between perpendiculars
L	N	Lift force
$LengthB$	m	Bulb Length
mx	$N.m$	Propeller torque
ν	m^2/s	Kinematic viscosity
N_{blades}	$-$	Number of blades
N_n	$-$	Number of collocation points in circumferential direction

Symbol	Unit	Explanation
n	rpm/rps	Propeller revolutions
P	$-$	Propeller pitch
$P_{0.7}/D_p$	$-$	Pitch ratio
ρ	kg/m^3	Density
Re	$-$	Reynolds number
R_{rudder}	N	Rudder axial force
R_T	$[N]$	Total Resistance
R_{total}	N	Ship resistance from OpenFoam
S	m^2	Rudder span
std	$-$	Standard deviation
S_w	m^2	Wetted surface area
ϑ	deg	Static trim
θ_{eff}	deg	Propeller skew
T	N	Thrust
t	m	Rudder thickness
t	$[-]$	Thrust deduction fraction
T_M	m	Mean draft
$ThicknessB$	m	Bulb Thickness
v_s	$-$	Ship speed [Kt or m/s]
X_1	m	Rudder stock position
X_{P2}	mm	Rotation axis in the twist function
XYZ	m	Rudder separation from propeller: longitudinally, laterally and vertically
$XposB$	m	Bulb longitudinal position
x_axis	$-$	Twist rotation axis in percentage of chord
ξ	$-$	Coverage, equal to the proportion of the rudder span in way of the propeller race
Y_{P1}	mm	Nose position in the twist function
Y_{total}	mm	Total rudder twist
Y_{Bottom}	mm	Rudder twist at Bottom side
Y_{sweep}	mm	Averaged rudder twist
Y_{Top}	mm	Rudder twist at Top side

Declaration of Authorship

I declare that this thesis and the work presented in it are my own and has been generated by me as the result of my own original research.

Where I have consulted the published work of others, this is always clearly attributed.

Where I have quoted from the work of others, the source is always given. With the exception of such quotations, this thesis is entirely my own work.

I have acknowledged all main sources of help.

Where the thesis is based on work done by myself jointly with others, I have made clear exactly what was done by others and what I have contributed myself.

This thesis contains no material that has been submitted previously, in whole or in part, for the award of any other academic degree or diploma.

I cede copyright of the thesis in favour of the University of Rostock.

Date Signature

1. Introduction

1.1. Motivation

Ship propulsion efficiency has been a very important matter of study, because it is directly related to the fuel consumption reduction or optimization. This problem is associated to hydrodynamics, because the flow induced by the propeller affects the operation of the rudder and thus the manoeuvrability of the entire ship.

The Energy Efficiency Design Index (*EEDI*) Regulations from *IMO* (*MEPC*) governs the rules that all new ships that are contracted after 1st of January 2013 have to follow. This requires most new ships to be 10% more efficient by 2015, 20% more efficient by 2020 and 30% more efficient from 2025. If implemented according to their time schedule, the *ICCT*[8] projects that up to 263 million tonnes (Mt) of CO2 will be reduced annually by 2030.

Since these regulations require a minimum energy efficiency for new ships, development of new technical improvements is continuously developed, especially in the components influencing the fuel efficiency. These components are known as Efficiency Improving Devices (*EID*), and are implemented in the propulsion system in order to improve the efficiency in the best way possible. There are different types of *EIDs*, for instance (among others):

- Appendages to reduce stern wave
- Air bubble on the bottom
- Fins in front of a propeller
- Special propellers
- Stators behind the propeller
- Rudder bulb
- Twisted leading edge of rudder

It is known that the twisted rudders can improve the propulsive efficiency of up to 2%. Twisted rudders in combination with rudder bulbs can improve propulsive efficiency even by up to 4%, this means that any improvement in this field is well accepted in the industry. It is assumed that the optimal rudder design depends on the propeller loading, thus the optimal rudder design might depend on the operational profile of the ship. This is a decisive point for the optimization, since a design optimized for one certain operating condition can be very sensitive with respect to changes in this condition.

The optimization of the rudder on the other hand is a process that can be developed even if the construction of the ship is already started, because the rudder is an exchangeable part that could be installed in any moment during the operating life of the vessel. Designs could be improved by hydrodynamic optimization procedure by means of numerical tools. Computational time and resources limit the economical feasibility of these methods. In the ship design field, the viscous flow around a ship can be approximated accurately using Reynolds-Averaged Navier-Stokes simulations (*RANS*).

However, when the rotating propeller is included, the computational demand is highly increased because of the high resolution grid requirements. A solution has been found by gathering the propeller blade forces from a potential flow simulation (Boundary Element Method – *BEM* as the most popular) and couple them as a force density source in the *RANS* simulation.

The coupled *RANS-BEM* method has been studied before. Typical applications study the interaction hull-propeller-rudder in different conditions. Most cases take the coupling in a time domain, either explicitly or implicitly. For example Sarasquete in [13] have done some CFD studies to assess the propulsive efficiency (for further optimization) using *RANS* simulations, taking a relatively short computational time. In the end they propose to use a coupled method for multiple case study, so the time for computation is even shorter for a set of designs.

1.2. Aim of this work

The main objective of this master thesis is to assess the optimization methodology of propulsion efficiency by means of two *EIDs*: twisted rudder and Costa bulb. This will be achieved by the implementation of a coupled method in which the propulsive efficiency is evaluated by a *RANS* (for the hull) and potential flow *BEM* (for the propeller) solver coupling. The rudder geometry is modelled with the Friendship framework (*CAESES*) which is coupled to a genetic like optimization strategy implemented in *FS-Optimizer* framework and the *RANS-BEM* solver.

A twisted shape will recover the rotational losses in the propeller slip stream for a specific propeller load. On the other hand a Costa bulb will reduce losses due to hub vortex. The

main design variables in the process chain are rudder twist and twist-axis, as well as bulb shape-size and position.

The coupled *RANS-BEM* method was developed by Schenke [14] in cooperation with the Fluid Engineering department of DNV GL SE Maritime Advisory division in Hamburg. This method was carried out with the aim to implement an interface between OpenFOAM *RANS* solver *simpleFoam* and *BEM* solver *PROCAL* developed by Maritime Research Institute of Netherlands (*MARIN*) in cooperation with Cooperative Research Ships Organization (*CRS*).

This method compared to other existing *RANS-BEM* couplings is focused on aspects such as: improvements of the force transfer procedure and the impact of the wake disc shape for the evaluation of velocities in the wake field. Since the disturbing ship hull in the *BEM* simulation is absent, this method requires an iterative update of inflow velocities for the *BEM* simulation and force densities for the *RANS* simulation.

On the other hand an optimization method will be implemented in order to analyse several geometries and get the best improvement of propulsive efficiency as possible. The tool used is *FS-Optimizer*, a framework developed at FutureShip GmbH. Optimization is performed by varying parameters (or design variables as mentioned) so that given objectives (thrust and torque) are met while constraints (twist angle range) are kept.

1.3. Outline of this work

Chapter 2 gives an overview of the theoretical background including the governing equations of the RANS and potential flow solvers, as well as information in rudder design and propulsive efficiency. Coupled simulation is described according to Schenke [14]. Then in Chapter 3 optimization method is further explained, detailing the parametric model creation in CAESES framework.

In Chapter 4 the mesh generation procedure is highlighted, then the set-up for the coupling scheme is described to finally make an analysis of mesh convergence.

In Chapter 5 the configuration of rudder without twist is studied, both with and without bulb to see its influence on the rudder characteristics. Initial results are presented as a starting point for the optimization procedure. In Section 5.1 the operating point for a rudder design is calculated in order to have a realistic propeller loading during the optimization procedure.

Finally in Chapter 6 the set-up of the optimization and final results of the analysis are presented, showing a design study for twisted rudder and bulb. In final Chapters 7 and 8, conclusions from this work are summarized providing some recommendations for further research on the topic.

2. Theoretical Background

This chapter gives a further explanation of the rudder design process and governing equations of the implemented model. Based on this background, the coupling method is explained at the end of this chapter.

2.1. Rudder design

The rudder, as described by Sarasquete [13], is a wing section with a hydrodynamic profile which pivots about a vertical axis. Normally it is located in the stern of the ship where redirects the flow of water coming from the propeller, producing a transverse force and turning moment about the ships' center of gravity. A rudder should be customized for each ship because choosing of geometric characteristics greatly influences its response in manoeuvring.

Regarding propulsive efficiency affected by the rudder, Tupper mentions in the book *Introduction to Naval Architecture*[16] that the energy of rotation in the propeller wake represents a loss of efficiency, therefore various ways are proposed for recovering this energy. One way is the rudder itself, which is designed so that the wake is diverted in slightly different directions above and below the propeller axis.

It is needed to distinguish the notation and particulars of the control surface, forces and centre of pressure. These characteristics are shown in Figures 2.1 and 2.2.

Main forces (lift and drag) are non-dimensionalised using the free-stream (ship wake) speed V, calculating coefficients as mentioned by Molland and Turnock [10]:

$$C_L = \frac{L}{\frac{1}{2}\rho A V^2}, \qquad C_D = \frac{d}{\frac{1}{2}\rho A V^2} \tag{2.1}$$

Normally presented in terms of the rudder incidence α:

$$C_N = C_L \cos\alpha + C_D \sin\alpha \tag{2.2}$$

Also, propeller thrust and torque coefficients are defined as:

$$K_T = \frac{T}{\rho n^2 D_p^4}, \qquad K_Q = \frac{Q}{\rho n^2 D_p^5} \tag{2.3}$$

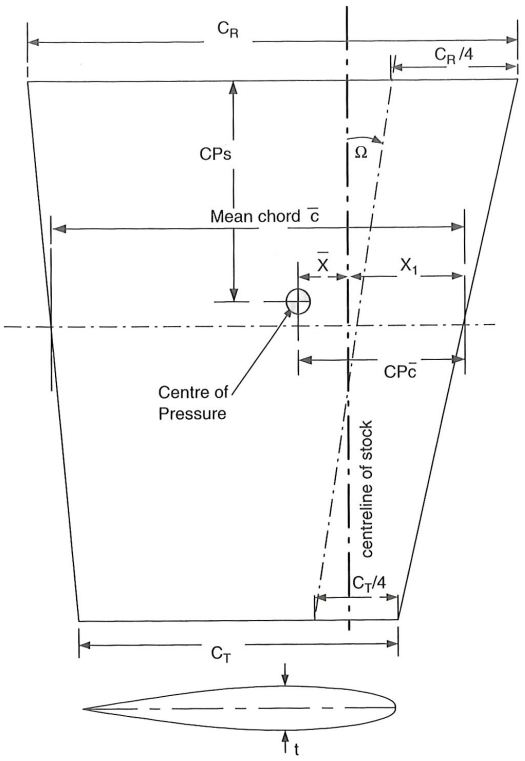

Figure 2.1.: Notation for typical all-movable control surface, [10]

In the design process it is important to be able to estimate the forces and moments for a particular rudder at a given angle of attack and inflow speed. Therefore in this work the lateral force (corresponding to lift) is measured as well as x direction (longitudinal) in order to optimize the design. Forces on the rudder are better explained in Figure 2.2.

2.1.1. Twisted Rudders

The rudder of a ship is a control device used to maintain or change the course of it, thus the main goal of designing this component is to maximize side control force while minimizing the drag or resistance. This is well explained by Turnock and Molland [17] as they examine how the design of the combined propeller-rudder system can maximise, up to some point, the propulsive efficiency without sacrificing the ability to manoeuvre.

A twisted rudder offers the opportunity to reduce cavitation risk on rudder sections by reducing effective angle of attack, although it is not the main objective of this master

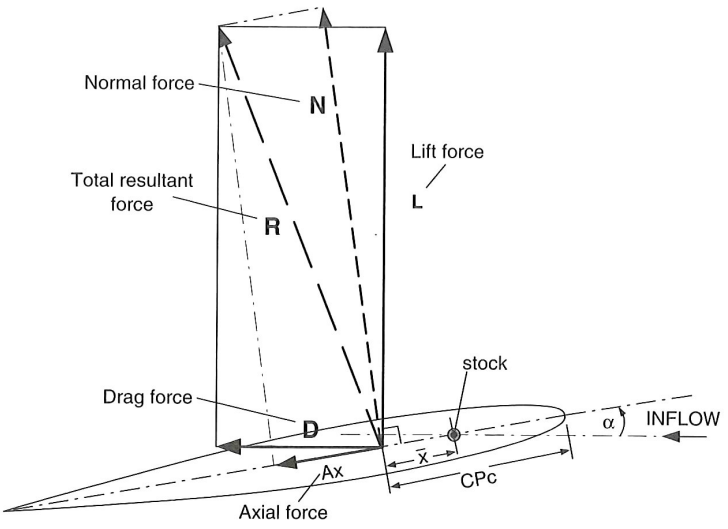

Figure 2.2.: Notation of forces and angles for all-movable control surface, [10]

thesis. It can also be used to alter effective thrust/drag of rudder by recovering rotational energy from propeller race. The purpose of applying a suitable twist for a zero rudder angle, is to have zero effective incidence and load across the span, as cited on [10].

Due to the rotational component of the propeller, conventional straight rudders at zero incidence encounter oblique flow angles to one side at the upper part and to the other side in the lower part. This behaviour creates opposing lift forces which (partially) cancel each other (but associated induced drag forces increase), as explained by Hochkirch and Bertram [7].

Furthermore, Mulland and Turnock [10] explain also that due to rotational nature of the slipstream, significant inflow angles are induced even at zero rudder incidence. In Figure 2.3 it is seen the effective incidence across the span for a typical service condition (advance ratio J=0.51) and an increase on thrust loading (J=0.35). Results reported by Mulland and Turnock [10] would suggest a variation in effective local incidence of up to about $\pm 9°$ for J=0.51 and $\pm 13°$ for J=0.35, due to a variation on the normal force coefficient C_N along the span.

High-efficiency rudders combine various approaches to save fuel, for example twisted rudders are combined with a bulb on the rudder as a streamlined continuation of the propeller hub.

In the present work twisted rudders are tested and compared by the results for: force generated by the rudder both axial and lateral (R_{rudder} and Fy_{rudder}), total ship resistance (R_{total}) and propeller torque (m_x) and thrust (T). In the optimization procedure the goal is to minimize the torque on the propeller shaft, since this is the factor that determines an increase or reduction in propulsive efficiency.

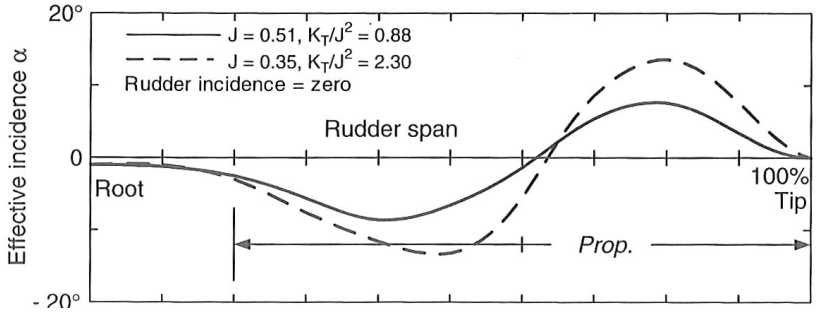

Figure 2.3.: Distribution of effective incidence across span at zero rudder angle, [10]

2.1.2. Rudder-Propeller-Hull interaction

Rudders are usually mounted downstream of the propeller to take advantage of the high speed flow induced by it, but on the other hand it imposes a swirl component, resulting on a complex flow arriving to the rudder. Similarly, the presence of the rudder also affects the flow passing through the propeller (thrust needs to be increased slightly due to the rudders presence), this means that the design of propulsion systems should include the design of propeller and rudder in order to increase the efficiency of the complete system. In Figure 2.4 it can further be seen the effect of the swirl, shifting local rudder incidence in one direction above propeller axis and other direction below the axis.

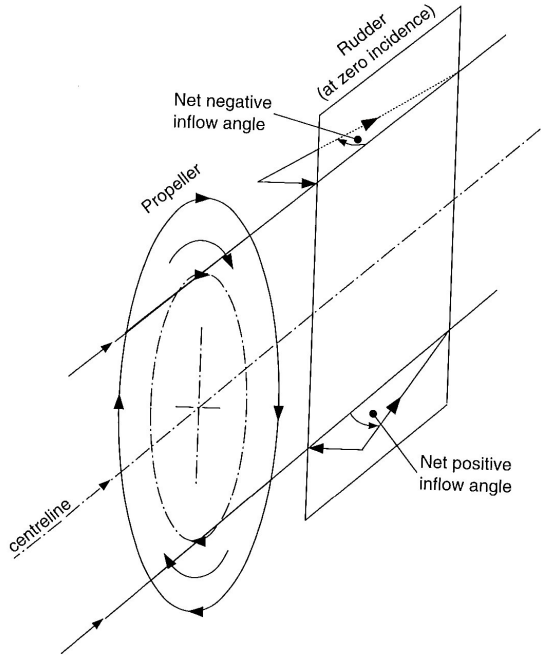

Figure 2.4.: Propeller-induced rudder incidence, [10]

It is important to recognize the parameters on which rudder forces depend in order to assess the interaction between rudder and propeller. Mulland and Turnock [10] divide them in four different categories to assess their effect on the rudder and propeller performance characteristics:

- *Flow variables*: include the time dependant variables and properties of the flow.
- *Rudder geometric variables*: Rudder incidence, span, mean chord, stock position, thickness, section shape, taper ratio, sweep and twist.
- *Propeller geometric variables*: diameter, pitch, blade area ratio, boss diameter, section shape, etc.
- *Relative position and size of the rudder and propeller.*

If these parameters are brought in non-dimensional form, the flow parameters become Reynolds number *Re* and advance ratio *J*. Then, if the basic geometric properties of propeller and rudder are kept fixed, the lift can be expressed as function of non-dimensional variables such as in Equation 2.4

$$C_L = f\left\{[J, Re, \beta], \left[\alpha, AR, \frac{X_1}{c}\right], \left[\frac{X}{D_p}, \frac{Y}{D_p}, \frac{Z}{D_p}, \xi\right]\right\} \tag{2.4}$$

The most important parameters (for a fixed propeller) are the propeller advance ratio J and rudder incidence α, since the geometric parameters will determine their influence on the performance of the rudder and propeller.

The velocity induced by the propeller on the rudder may be calculated using axial momentum theory, which is deeply explained by Mulland and Turnock [10, ch3.6].The propeller is considered as an actuator disc, capable of imparting axial motion to a fluid. After solving a system using Bernoulli‘s equation upstream and downstream, it can be shown that:

$$\frac{2T}{\rho A_1} = \frac{8K_T}{\pi J^2} V_0^2 \tag{2.5}$$

Where $K_T = T/\rho n^2 D_p^4$ and $J = V_0/nD_p$

At the end it is found (Equation 2.6) that the propeller-induced velocity arriving at the rudder is a function of the propeller thrust loading K_T/J^2, Equation 2.5 and distance X between the propeller and rudder. Then logically, increasing the propeller thrust loading, the induced velocity also increases.

$$V_R = V_0\left[1 + K_R\left\{\left[1 + \frac{8K_T}{\pi J^2}\right]^{1/2} - 1\right\}\right] \tag{2.6}$$

Where K_R (Equation 2.7) is a *Gutsche*-type correction based on the distance of the rudder from the propeller (X).

$$K_R = 0.5 + \frac{0.5}{[1 + (0.15/(X/D_p))]} \tag{2.7}$$

Using continuity of flow the diameter of slipstream of the propeller is found as:

$$\frac{D_R}{D_p} = \frac{\left[[1 + (8K_T/\pi J^2)]^{1/2} + 1\right]^{1/2}}{\left[2\left\{1 + K_R\left\{[1 + (8K_T/\pi J^2)]^{1/2} - 1\right\}\right\}\right]^{1/2}} \tag{2.8}$$

Equations 2.6 and 2.8 can be used as a first idealised approach of the slipstream on the rudder. In reality, inflow to the propeller is non-uniform and the propeller-induced velocity is also non-uniform over the blade radius.

The hull presence also influences the system in great manner, since it slows down the inflow to the propeller and rudder. The hull affects the inflow angle as well, it has flow-straightening effects. The wake (or effective speed) into the propeller is calculated by the coupled *RANS-BEM* method and further explained chapter 3.

2.2. Propulsive efficiency

"When a body moves through a fluid it experiences forces opposing the motion" Tupper [16]. For a ship it is affected by both air and water forces, having an interface in-between (free surface). Since no free surface simulations where conducted, the free surface contribution to resistance (governed by the ratio between inertial and gravitational forces: Froude number) is obtained by the aid of experimental data.

When performing a simple hydrodynamic analysis as the one shown by Tupper [16], the following non-dimensional combinations are likely to be significant:

$$\frac{R}{\rho V^2 L^2}, \qquad VL\frac{\rho}{\mu}, \qquad \frac{V}{\sqrt[2]{gL}}, \qquad \frac{P}{\rho V^2}, \tag{2.9}$$

The first three ratios are the most relevant for the present work, are respectively, the resistance coefficient, Reynold's number and Froude number. The fourth is related to cavitation.

The determination of the propulsion efficiency for a model scale container ship based on the coupled simulation is explained in following steps, cited from Schenke [14]. Any experimental data used in this work is obtained from resistance and propulsion test results

provided by *Schiffbau-Versuchsanstalt Potsdam* (*SVA*) [11]. The procedure for the determination of the free surface resistance based on the model test results is cited from Herbel [6].

It is assumed that the overall resistance R_T as measured during a resistance test can be decomposed into three contributions, namely friction R_{fric}, viscous pressure R_{press} and free surface resistance R_{FS}:

$$R_T = \underbrace{R_{\text{fric}} + R_{\text{press}}}_{R_{DB}} + R_{FS} \tag{2.10}$$

The first two terms in Equation (2.10) can be determined by a double body *RANS* simulation, therefore they can be combined. The free surface contribution is obtained by subtracting the double body resistance from the total experimental resistance:

$$R_{FS} = R_T - R_{DB} \tag{2.11}$$

Schenke [14] explains the determination of the operating point by taking the desired ship velocity as constant inflow velocity in the *RANS* simulation. The free surface resistance can be considered as constant too. To allow for comparison between the experimental and numerical operating point, friction deduction has to be taken into account in the numerical simulation as well.

The friction deduction F_D is meant to compensate the overestimation of frictional resistance during the model scale resistance test compared to the frictional resistance of the full scale hull. It is calculated according to the SVA test [11] as:

$$F_D = \frac{1}{2} \cdot \rho_m \cdot S_m \cdot V_{a_m}^2 \cdot [C_{F_{mC}} - (C_{F_s} + \Delta C_F)] \tag{2.12}$$

Where $C_{F_{mC}}$ is the total resistance coefficient at the temperature of the self-propulsion test, ΔC_F is the roughness allowance and the indices m and s denote the model and full scale ship parameters respectively.

Based on these considerations the total resistance R_{TP} under self propulsion conditions is obtained by the sum of calculated double body resistance R_{OF} (from OpenFoam results) and free surface resistance R_{FS}, minus the friction deduction [6]:

$$R_{TP} = R_{OF} + R_{FS} - F_D \tag{2.13}$$

The propeller rotation is then varied until an equilibrium between ship resistance and propeller thrust is obtained:

$$T = -R_{TP} \tag{2.14}$$

The sign of R_{TP} infers that propeller thrust and resistance point in opposite directions. Also note that the suction of the propeller is already included in the resistance component R_{OF}, since it results from a pressure integration over the hull under self propulsion conditions.

One can finally determine the propulsion efficiency η_D for the model scale ship at the operating point as follows:

$$\eta_D = \frac{P_E}{P_D} = \frac{(R_T - F_D)\, v_s}{2\pi Q n} \tag{2.15}$$

In Equation (2.15) P_E denotes the effective power from [11], where v_s represents the model scale ship speed and $R_T - F_D$ represents the corresponding resistance as measured during the resistance test minus friction deduction. P_D denotes the power delivered to the propeller at the operating point, where n and Q represent the corresponding rotational rate and propeller torque (same as m_x in further chapters). This delivered power has a high importance in the optimization procedure, since a reduction on this value means an increase on overall propulsion efficiency. Thus the optimization objective is more related to minimize P_D.

Since the resistance R_T obtained from the resistance test in [11], is taken as reference to calculate the free surface contribution R_{FS}, it is implicitly assumed that R_T is the same for experimental tests, coupled simulation and full *RANS* simulation. This means that the effective power P_E for a given ship speed is the same for all three methods as well.

However, since the present is the development of an optimization procedure, several rudder designs are to be simulated by means of the coupled method, moreover each design would be affected by different free surface resistance. Thus the aforementioned assumption induces an error on the results, because in order to simplify the process, R_{FS} is obtained from an initial design (same used for the mesh study). This error is assumed small enough to not to affect the results significantly.

2.3. Coupled Scheme

The simulation is to be performed by the use of a coupled *RANS-BEM* method developed by Schenke [14] implementing an interface between the OpenFOAM *RANS* solver (Automated by Herbel [6]) *simpleFoam* and the *BEM* solver *PROCAL*. The basic background theory on Potential flow theory and RANS equations is presented in following sections.

2.3.1. Potential Flow

The basic principle of the panel method, as described by Molland and Turnock in [10] is based on the linear superposition of source/sinks, vortices and/or doublet elements over the lifting surface, such that the boundary conditions are satisfied on the body, across the wake and in the far field.

The potential flow equations in which *PROCAL* is based on are presented by Katz and Plotkin in [9]. Schenke [14] summarizes the equations in order to make a better description of the method, presented below.

The total potential Φ of the considered domain, defined in [9] can be subdivided into a potential ϕ_∞, which represents the potential of the free stream inflow velocity $\mathbf{v}_\infty$, and a potential ϕ representing the disturbance due to the circulated body:

$$\Phi = \phi + \phi_\infty \tag{2.16}$$

Considering a body with known boundaries S_B, submerged in a potential flow, as shown in Figure 2.5. The flow of interest is in the outer region V where the incompressible, irrotational continuity equation, in the body's frame of reference in terms of the total potential Φ^* is:

$$\Delta^2 \Phi^* = 0 \tag{2.17}$$

Based on *Green's identity* the disturbance potential ϕ is represented as follows [9, ch9]:

$$\phi = \frac{1}{4\pi} \int_{S_b} \left[\mu \mathbf{n} \cdot \nabla \left(\frac{1}{|\mathbf{x} - \mathbf{x_0}|} \right) - \sigma \frac{1}{|\mathbf{x} - \mathbf{x_0}|} \right] \mathrm{d}S + \frac{1}{4\pi} \int_{S_w} \left[\mu_w \mathbf{n} \cdot \nabla \left(\frac{1}{|\mathbf{x} - \mathbf{x_0}|} \right) \right] \mathrm{d}S \tag{2.18}$$

In Equation 2.18, as per Schenke [14] μ and σ denote the dipole and source strengths at location $\mathbf{x}_0$ on the surface S_b of the circulated body. Analogous μ_w denotes the dipole strength at location $\mathbf{x_0}$ of the wake sheet. The normal vector of S_b and S_w at location $\mathbf{x}_0$ is represented by $\mathbf{n}$. Vector $\mathbf{x}$ denotes an arbitrary point in the flow field. The unknowns μ, σ and μ_w can be solved numerically by setting the following boundary conditions:

- First boundary condition, also referred to as the *Neumann Boundary Condition*, states that the flow normal to the solid surface S_b must be equal to zero [9, ch9]:

$$\mathbf{n} \cdot (\nabla \phi + \mathbf{v}_\infty) = 0 \tag{2.19}$$

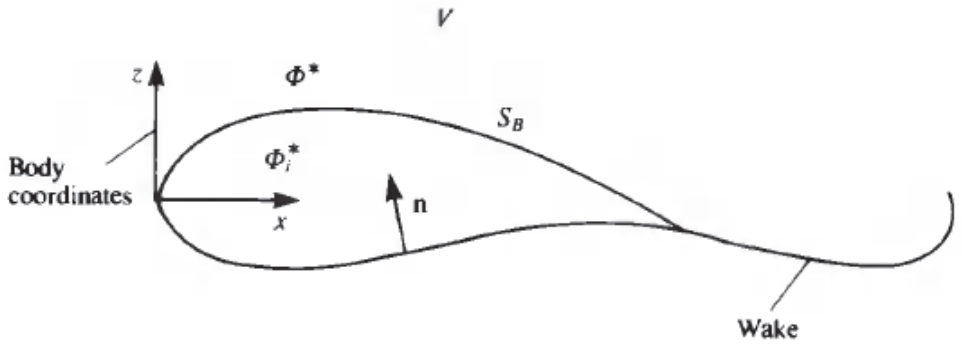

Figure 2.5.: Potential flow over a closed body [9, ch9]

- Second boundary condition states that the impact of the disturbance potential vanishes far from the disturbing body [9, ch9]:

$$\lim_{|\mathbf{x}-\mathbf{x_0}|\to\infty} \nabla\phi = \mathbf{0} \tag{2.20}$$

- Third condition sets the wake dipole strength at the trailing edge. In combination with the specification of the wake shape it provides the *wake model*. It states that the dipole strength of the wake at the trailing edge equals the potential difference between the upper and the lower side of the trailing edge, represented by μ_U and μ_L respectively [9, ch9]:

$$\mu_w = \mu_U - \mu_L \tag{2.21}$$

Schenke [14] also explains that once the potential flow problem is solved, induced velocities can be calculated by *PROCAL* based on the given dipole and source strengths. It is distinguished between a near field and a far field evaluation of induced velocities, where in the far field case the panel element is represented by a point singularity. The near field formulation, in contrast, assumes a surface distribution of the dipole or source strength.

Typically the far field formulation can be applied if the distance between point x and the panel centre at x_0 exceeds 3-5 times the average panel diameter [9, ch9]. In this work the application of the simplified far field formulation will be valid in the majority of considered cases. Further information on the evaluation of induced velocities is given in the *PROCAL* manual [2] and Low speed aerodynamics book [9].

2.3.2. RANS Equations

A detailed description of the *Navier-Stokes* equation ca be found in [9, ch1].In this section the summary presented by Schenke [14] is mentioned. The *Navier-Stokes* equation for an incompressible single phase flow is given in Equation 2.22.

$$\frac{\partial \mathbf{v}}{\partial t} + (\mathbf{v} \cdot \nabla)\,\mathbf{v} = -\frac{\nabla p}{\rho} + \nabla\,(\nu \nabla \cdot \mathbf{v}) + \frac{\mathbf{f}}{\rho} \tag{2.22}$$

Where v denotes the fluid velocity, p the pressure, ρ the fluid density and ν the kinematic viscosity. Finally f represents a source.

To obtain a steady state solution the time derivative term in Equation (2.22) is cancelled out. The default formulation of the *Navier-Stokes* equation for the *simpleFoam* solver does not include any external sources. In combination with the continuity equation for an incompressible single phase flow this leaves the following governing equations for the *simpleFoam* solver.

$$\nabla \cdot \mathbf{v} = 0 \tag{2.23}$$

$$(\mathbf{v} \cdot \nabla)\,\mathbf{v} = -\frac{\nabla p}{\rho} + \nabla\,(\nu \nabla \cdot \mathbf{v}) \tag{2.24}$$

Schenke [14] has modified Equation (2.24) by adding a force density term f to the momentum, which reflects the impact of the propeller:

$$(\mathbf{v} \cdot \nabla)\,\mathbf{v} = -\frac{\nabla p}{\rho} + \nabla\,(\nu \nabla \cdot \mathbf{v}) + \frac{\mathbf{f}}{\rho} \tag{2.25}$$

The determination of the source term f in Equation (2.25) at each coupling step, is of great importance in the method, because it includes the conversion of propeller blade forces into force density sources for the RANS mesh. How the continuity equation and the *Navier-Stokes* equation for an incompressible single phase flow are solved by the *SIMPLE* algorithm is explained in [3] by Capelli and Mansour. Turbulence is accounted for using the $k - \omega - SST$ model, whose implementation in OpenFoam is described in detail by Nilsson and Gyllenram in [12].

2.4. Coupled Simulation

Figure 2.6 visualises the information flow between the potential flow (*BEM*) solver *PROCAL* and the *RANS* solver OpenFoam.

This process is explained by Schenke [14]. Starting with an open water propeller simulation, the potential flow solver yields the blade panel forces for a free stream inflow velocity v_∞, which is associated with the free stream potential ϕ_∞ (Equation (2.16)). The blade panel forces are part of the *PROCAL* output, obtained by multiplying the pressures of

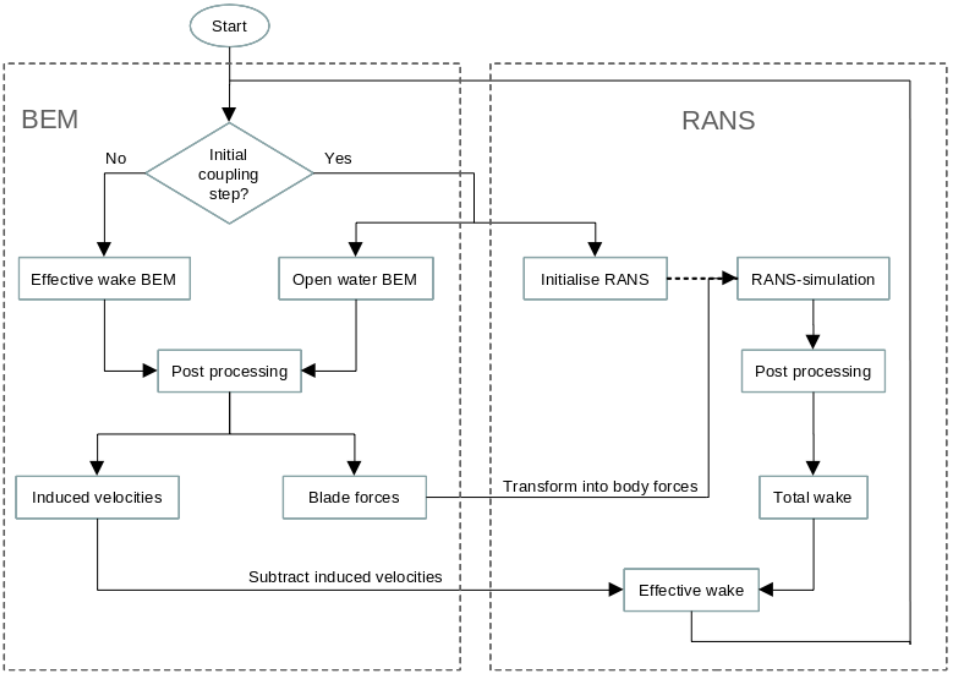

Figure 2.6.: Coupling scheme, [14]

the surface panels with the corresponding areas and then interpolating the surface forces to the camber surface of the blade.

The resulting discrete forces are transferred to a stationary domain: the *propeller disc*. The stationary force field is obtained by tracing a single blade for the duration of one complete revolution to preserve the main characteristics of the original force field. The stationary force field in the propeller disc is then transferred to the *RANS* mesh, which involves a conversion into volume force densities, also referred to as body forces. The volume force densities dF/dV are added as a source term to the *Navier-Stokes* equation (Equation (2.24)).

In the first coupling step, initial *RANS* simulation is conducted with the body forces obtained from the open water potential flow simulation. The resulting velocity field is the input of the subsequent potential flow simulation, meaning that v_∞ now represents the ship wake, which is assumed as constant in direction of the propeller axis.

Schenke [14] clarifies that the velocity field obtained by the *RANS* simulation (*total wake field*) implicitly contains the velocity contribution induced by the propeller, which must be subtracted. It happens that the induced velocities can not directly be extracted from *RANS* solution, but they can be obtained from the previous potential flow solution. Therefore, the new potential flow input at coupling step $i+1$ is given by Equation 2.26.

$$v_{\infty,i+1} = v_{\mathrm{RANS},i} - v_{\mathrm{ind},i} \tag{2.26}$$

This relation (the total wake field minus the propeller induced velocities) is the *effective wake*. To be consistent with the stationary approach, induced velocities are averaged in time. The circumstance that the propeller load and its inflow interact with each other, requires for an iterative update of effective inflow on the potential flow side and body forces on the *RANS* side until convergence of the effective wake and propeller forces is achieved, this is known as *effective wake coupling*.

2.4.1. Mesh Coupling

The OpenFOAM routine `topoSet` is used by Schenke [14] to create a geometrical shape (cylinder in this case) enclosing the propeller and a set of cells whose centres are located in the interior of the geometry. This enclosure is the area for transfer of forces in the *RANS* mesh. User should input the cylinder radius and two points specifying its axis.

Then the induced velocities and blade forces obtained by the potential flow simulation are transferred to the stationary domain. This is done in every coupling step, it means that the stationary induced velocity field is subtracted from the stationary total wake field obtained by the *RANS* solver (Equation 2.26), which provides the flow input for the subsequent potential flow simulation.

Schenke [14, ch 3.4] explains also how both total and induced velocities are evaluated in a wake disc located upstream of the propeller. He states that at each position in the wake disc, the stationary induced velocity is represented by its mean value in time, resulting from the contributions at each time step during one revolution.

The force transfer starts with a force interpolation using *Fast Fourier Transformations (FFT)*, then some mathematical approaches and a correction for the conservation of stationary force and torque are applied. Each discrete force F_S at coordinate x_S is now transferred to a set of neighbour cells in the *RANS* mesh. This cell set is given by the quantity of cells whose cell centres are located in the interior of a sphere S with radius R_S (see Figure 2.7).

The total volume of cells within S is denoted by V_S and the corresponding number of cells is denoted by N_S. Forces, volumes and cell centre coordinates attached to the single cells inside S are denoted by F_i, V_i and x_i respectively. Finally, the distribution of force is done when it fullfils some requiremens defined by Schenke [14, ch 3.5] regarding: Force distribution (function to guarantee smooth transitions at the intersection of overlapping spheres), Force density (uniform within S, assuming the distribution function for a single propeller disc force as constant) and force (and torque) conservation.

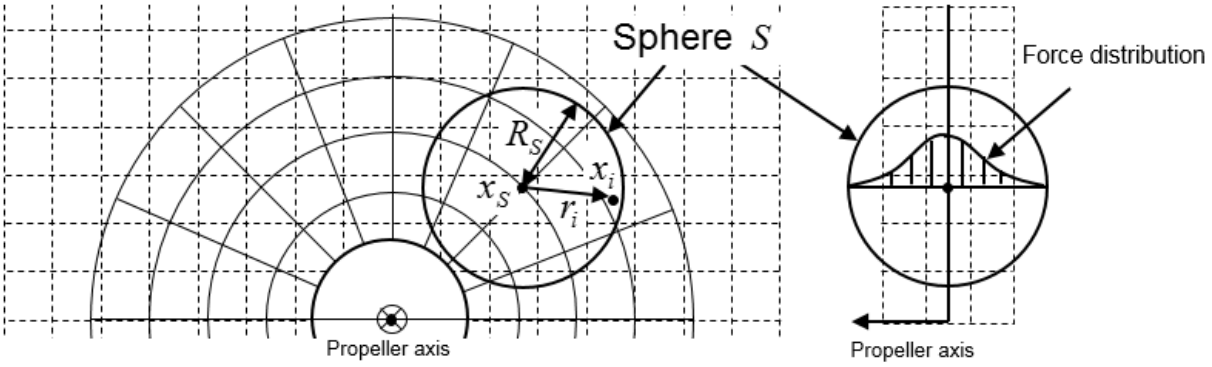

Figure 2.7.: Transfer of stationary blade forces, [14, ch 3.5]

2.4.2. Convergence of Coupling Steps

Schenke [14] has derived a criterion based on which subsequent coupling steps are initiated. Calculation time of the potential flow solver is small compared to that of the *RANS* solver and it is always run until its internal convergence criterion is satisfied. Therefore the criterion is for the current *RANS* solution to be considered as accurate enough to initiate the next coupling step.

It is emphasized that if the current *RANS* simulation is run for too long, the overall number of *RANS* iteration steps gets very large. At the same time, if the coupling is initiated too early, the time gain due the smaller number of iteration steps is counterbalanced by the extra time it takes to finalise the simulations and perform post-processing routines.

An example of convergence is presented in Figure 2.8 which includes multiple coupling steps. It shows the progress of combined hull and rudder forces versus the iteration step for a rotational rate of $12.33s^{-1}$ for the ship model velocity of $v_s = 1.6686m/s$, run for the mesh Fine22 (used in the mesh study shown in Chapter 4.1). According to the figure convergence of combined hull and rudder force is achieved at approximately 2500 iteration steps. In the present study, the convergence is analysed especially for the rudder forces.

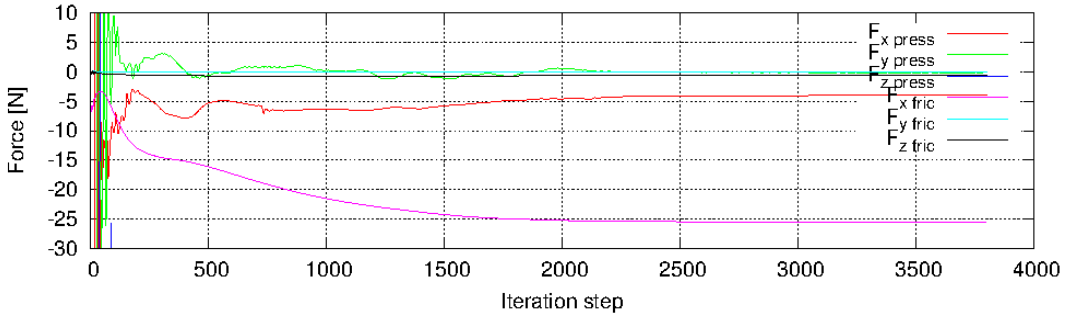

Figure 2.8.: Convergence of combined hull and rudder forces for mesh Fine22

The criterion assumed by Schenke [14] is that the current *RANS* solution is sufficiently accurate to initiate the next coupling step if the velocity field within the propeller cell set has reached a local convergence criterion. The velocity residual within the propeller cell set is expressed in terms of the velocity field deviation between two subsequent iteration steps: j and $j-1$. The deviation is measured by the sum of squared deviations over the propeller cell set, where N_c denotes the number of *RANS* cells in the set:

$$\varepsilon_j = \sum_{i=1}^{N_c} \left(v_i^j - v_i^{j-1}\right)^2 \tag{2.27}$$

According to this, it is expected that ε_j will decrease with an increasing number of iterations and end up in an oscillation around a residual value (see Figure 2.9). However, neither the residual value of ε_j nor the oscillation amplitude are known. The peaks indicate each coupling step, since the variation of the force density distribution in the propeller cell set imposes a disturbance on the *RANS* solver.

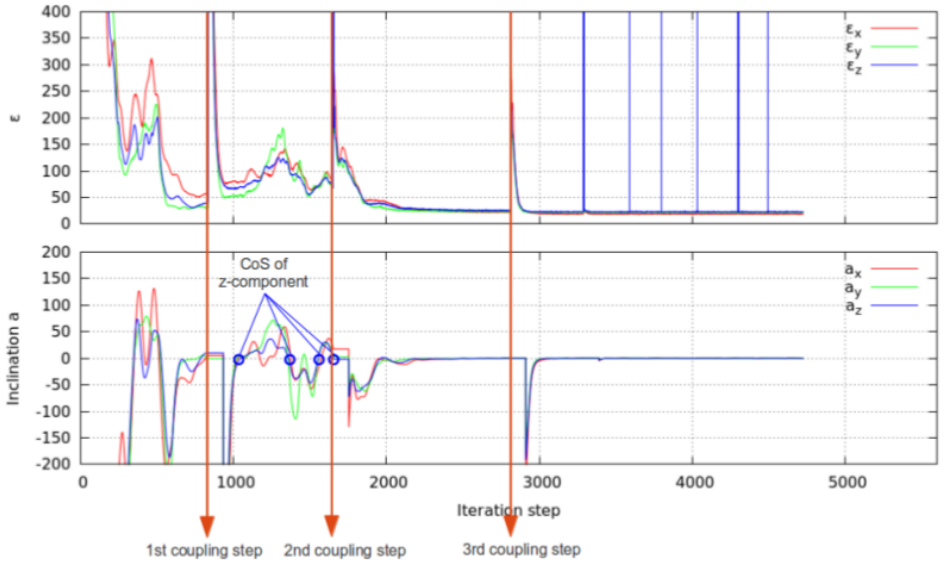

Figure 2.9.: Progression of the local velocity residual (upper figure) and progression of its statistically averaged sloped (lower figure) with CoS (change of sign) [15]

Schenke [14] takes another aspect into account to undergo the convergence criteria, it is reflected by the progression of the statistically averaged inclination a of the residual. It is now assumed that the current solution has converged to sufficient extent if the inclination a has changed its sign by a specific amount, that should be 3 or larger. With an increasing number of coupling steps the impact of the disturbance introduced by the coupling step initiation on the inclination tends to decrease.

However, the example presented in Figures 2.8 and 2.9 the simulation is stopped until the number of coupling steps is reached (user defined), normally around 7 coupling steps

should be sufficient for an overall convergence of the method, because this coupling scheme does not implement an overall convergence criteria, which would be recommended to apply in further research.

3. Method Description

This chapter is an overview of the optimization method assessed in the present work. It contains basically a summary of the method loop in the FS-Optimizer framework, general description of the parametric CAD generation with CAESES framework and data collection depiction.

In general, optimization is the search and selection of a best element regarding some criteria, from a set of variable alternatives. An optimization problem consists then in minimizing a real function. Every process has its own needs of optimization, meaning minimizing different characteristics, this is known as multi-objective optimization. Numerous optimization methods have been developed to solve problems, and every algorithm has its advantages and drawbacks because their abilities depend on the problem itself, constraints, objectives and behaviour of cost function.

Algorithms can be divided basically in 2 parts: Deterministic and Stochastic. The deterministic methods are based on the cost function or its derivatives, have a high convergence rate but depend on the starting point of the algorithm. Examples of this method are: Newton-Raphson, Golden search, Descend method, SIMPLEX and Geometric method. On the other hand, the stochastic methods are based on probabilistic laws and have random convergence with a low rate, but may as well depend on the starting point of the algorithm. Examples are: Montecarlo, Tabu and Genetic algorithm.

The work highlighted in this thesis needs a first step of generating a geometry according to the variables selection. A simulation of this design is run with the coupled method. Resulting data is collected and compared to baseline or other designs. Finally the objective function is studied, in order to select variables again and generate a new rudder geometry. The loop will finish when the algorithm criteria is achieved (selected number of designs).

In Section 3.1, the general description of this method is presented, algorithms used are described according to the literature. Parametric CAD modelling is shown in Section 3.2. Finally in Section 3.3, the process of data collection using scripts is described.

3.1. Optimization method

FS-Optimizer is an integration platform for multi-objective optimization, uses a graphical user interface and algorithms (like Brent, Newthon Raphson, SOBOL, Non-dominated Sorting Genetic Algorithms and more) to solve optimization problems.

A loop is defined by the user in the process chain, where all the jobs, functions and constants are defined in a given order. In the algorithm section, user might select and activate all the methods to use. Variables are defined and activated from the beginning and finally objective functions and constraints depend on the values defined before.

3.1.1. Process chain

The process followed by the present optimization is explained in Figure 3.1, where red boxes indicate the beginning and end of the total procedure, green boxes denote a sub-process inside the optimization (algorithm selection and coupled *RANS-BEM* method).

FS-Optimizer starts a process chain by the selection of an algorithm (Sobol or NSGA-II based), then designs are created in a new directory (with the algorithm name). To generate the parametric CAD, variables are selected (for rudder or bulb). A new sub-directory is created with the design name, in which the geometry is generated by CAESES framework and meshed with Star-CCM+ (see Section 3.2 and Chapter 4).

After mesh is created, simulation resources files are copied in order to start the coupled method for each design. Results are obtained thanks to the scripts folder (see Section 3.3). At this point, objectives are analysed. If algorithm finishes, the optimization ends, otherwise a set of variables is chosen and a new loop started.

3.1.2. Algorithm selection

In present optimization procedure, mainly two algorithms are used: Sobol and NSGA-II based. The selection of each algorithm depends on the user preferences as well as accuracy and computational effort of each method.

Sobol

The Sobol algorithm is used to generate a so called *DOE* (design of experiments) tables. Exploration DOEs are very effective to gather information about the optimization problem at hand and about the whole design space. In present cases the DOE database is searched

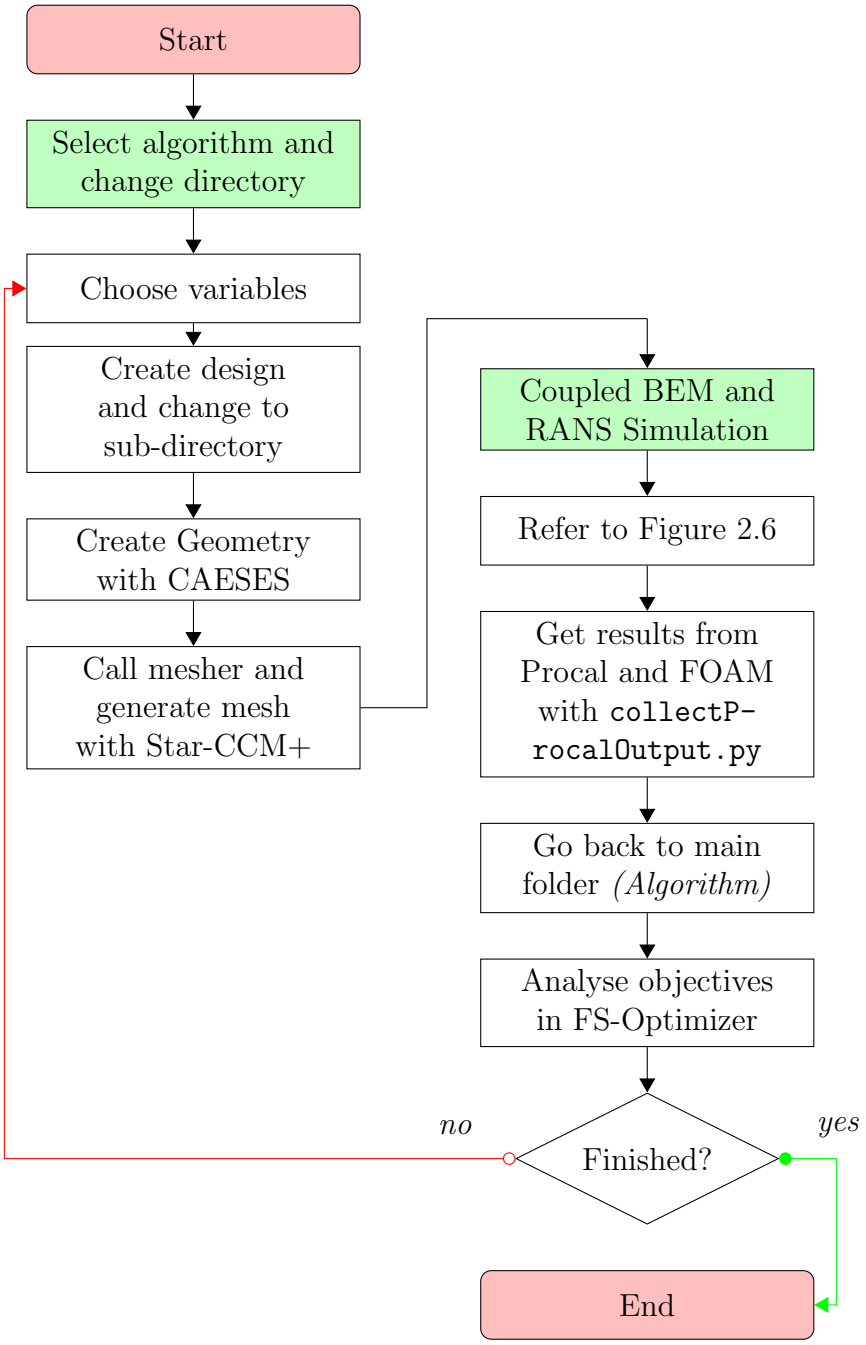

Figure 3.1.: Optimization flowchart

to detect a suitable starting point for a subsequent focused genetic based optimization process.

As described in the FS-Optimizer manual [5] number sequences like the Sobol sequence are sometimes called quasi-random or low discrepancy sequences. Such a sequence is "less random" than a (pseudo-)random number sequence, which spread points randomly in design space (bullet points), but shows to be more effective, e.g., in global optimiza-

tion tasks. This is because low discrepancy sequences tend to sample the design space more uniformly than random numbers. Basically, Sobol is a deterministic algorithm that imitates the behaviour of a random sequence. Similar to random number sequences the aim is a uniform sampling of the design space. But in this case the clustering effects of random sequences are reduced.

NSGA-II based

Genetic Algorithm (GA) cited from the FS-Optimizer manual [5], is a stochastic population-based optimization method that simulates the principle of natural evolution involving survival of the fittest individuals over generations. New individuals are created by interchanging genetic material of their parents (previous solutions) through genetic operations such as crossover and mutation. These genetic operations can be adjusted to guide the search toward the global optimum.

The resultant NSGA is based on the NSGA-II developed by Kalyanmoy Deb [4]. First, individuals are assigned a rank according to the non-dominated front to which they belong. The first front being completely non-dominant set in the current population and the second front being dominated only by the individuals in the first front and the front goes so on..

```
fast-non-dominated-sort(P)
for each p ∈ P
  S_p = ∅
  n_p = 0
  for each q ∈ P
    if (p ≺ q) then                    If p dominates q
      S_p = S_p ∪ {q}                  Add q to the set of solutions dominated by p
    else if (q ≺ p) then
      n_p = n_p + 1                    Increment the domination counter of p
  if n_p = 0 then                      p belongs to the first front
    p_rank = 1
    F_1 = F_1 ∪ {p}
i = 1                                  Initialize the front counter
while F_i ≠ ∅
  Q = ∅                                Used to store the members of the next front
  for each p ∈ F_i
    for each q ∈ S_p
      n_q = n_q − 1
      if n_q = 0 then                  q belongs to the next front
        q_rank = i + 1
        Q = Q ∪ {q}
  i = i + 1
  F_i = Q
```

Figure 3.2.: NSGA-II Non-dominated sort [4]

To spread the solutions along the front at each new generation, a crowding operator is implemented. Parents are selected from the population by using binary tournament selection based on the rank and crowding distance. In Figure 3.2 it is seen how the algorithm is sorted for every individuals in main popullation P. For a better understanding of the algorithm, it is recommended to read the article presented by Kalyanmoy Deb [4].

3.1.3. Objective function definition

The majority of real life problems need to account for multiple objectives, for example in the case of the twisted rudder optimization the objectives could be: minimize the ship resistance at certain speed, increase the propeller thrust (for same loading), minimize the propeller torque and revolutions (delivered power), minimize the lateral force (lift) by the rudder or minimize the cavitation probability. Objective selection is further discused in Chapter 6.

The selection of objectives rely upon the user needs and criteria. This is a crucial point for the optimization procedure, since from this objective function the algorithm will behave in order to look for an optimum result in the variable selection. When analysing more than one objective, it is important to check the so-called *Pareto* frontier and look up the best result according to the requirements.

There are also some different methodologies for the multi-objective assessment. For instance in this work, the weighting method is used, which consist in giving a weight factor for each objective to compile them in a unique objective function $f(x)$.

The final assessment of this optimization is to run with a double objective function, based on minimizing rudder longitudinal force (R_{rudder}) and reducing the total propeller delivered power ($P_D = 2\pi Qn$), which is inversely proportional to the total propulsion efficiency (η_D).

3.2. Parametric CAD model - for twisted rudder

The twisted rudder is modeled in CAESES (Friendship framework) by the use of parametric functions. An example of the rudder model is shown in Figure 3.3, which has a twist angle of -10° at the top and 10° at the bottom, at a rotation axis located at 30% of the chord length. On the other hand, the Costa bulb is a revolution geometry based on a *NACA* profile with a real scale chord of 7.5 m, longitudinal position 0.1 m in front of the rudder and thickness 0.23 of the chord. These properties are not changed in initial rudder studies (see Section 6.1 and 6.2), but are varied in further study in order to optimize bulb size and position (see Section 6.3).

As it is shown in Figure 3.4, the variables in the parametric functions control the geometrical properties of the model such as: twist angle and axis, chord, thickness, taper ("LE position", allocates the leading edge forth and back) and height. These functions are represented from bottom to top of the rudder, having different control points along rudder's height. These points are considered as parameters by the optimization procedure, then in this work twist angle offset points and rotation axis, as well as the bulb thickness, length and position are the user input variables that will control *FS-Optimizer* process chain.

Figure 3.3.: Twisted Rudder modelled in CAESES framework

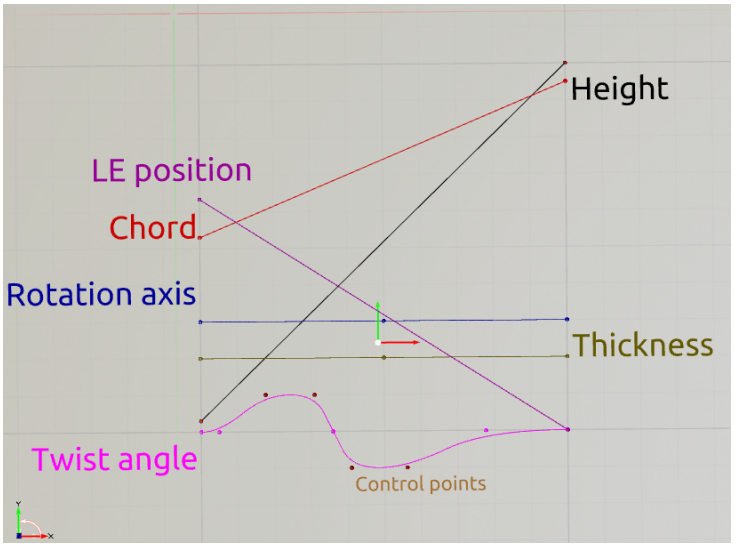

Figure 3.4.: Parametric functions for rudder modelling in CAESES framework

Since twisting the rudder depends on the height, as well as the chord, this value is another important factor to take into account. In order to solve this as a mathematical expression, a feature definition is created to influence the twist of the profile according to the functions already created (angle, rotation axis and chord). Then Equation 3.1 represents the nose position (Y_{P1}) when selecting an angle α and twist axis X_{P2} for every chord length c along rudder's height.

$$Y_{P1} = tan(\alpha) X_{P2} C \tag{3.1}$$

It is seen in Figure 3.5 that for the same twist angle (α and $-\alpha$), different twist is obtained (Y_{P1}) if the axis X_{P2} varies (from 0.3 red graph to 0.2 blue graph), thus the behaviour of the surrounding flow also differs. This means that in order to have a better control of the variables, the monitoring feature in the *FS-Optimizer* is Y_{P1} (for the chord length of

maximum twist at top and bottom), which relates the angle with the rotation axis as a unique function, although the user introduces them separately.

In the same manner, the bulb is created as a revolution geometry based on a *NACA* profile with maximum camber at 20% of the chord. It is also possible to take thickness and length (case 0.23 and 7.5m in real scale, for initial calculations) to be optimization parameters. Bulb position is another factor to bear in mind since it might affect the generation of hub vortex (thus influences the rudder resistance). Therefore its position with respect to hub cap is taken as design parameter for the last optimization run, since initial procedures are run with a fixed position of 0.1 m (in front of rudder) as presented in Chapter 6.3.

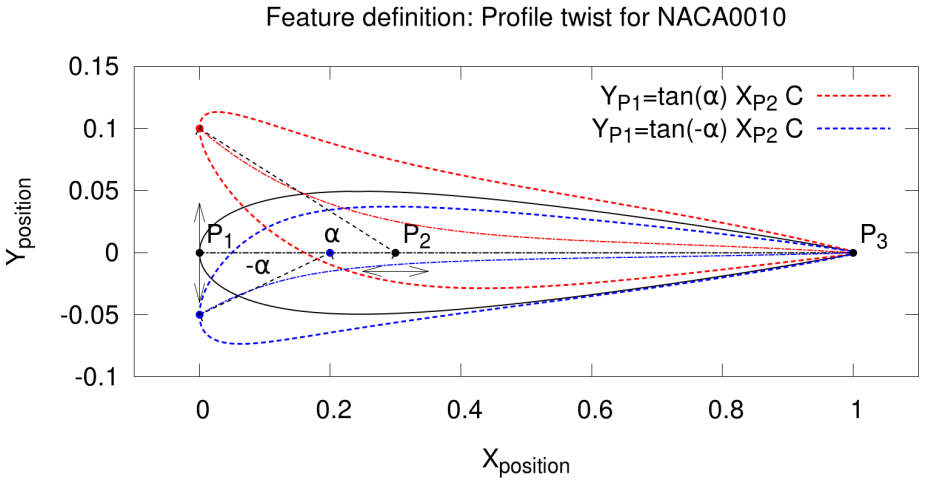

Figure 3.5.: Parametric functions for rudder modelling in CAESES framework

Two other parametric geometries are created additionally in order to generate a refinement around the leading edge of rudder and bulb. These geometries are both cylinders, one along the leading edge which varies accordingly with the twist angle function and another-one which varies with the thickness and position of the bulb (see Figure 3.6).

Finally in Figure 3.7 a *CAESES* script `twist.fsc` is presented, which creates the parametric geometry and exports the `.stl` files shown in Figure 3.6. The variables are represented as $\$ang\_b\$$, $\$ang\_t\$$, $\$x\_axis\$$ for the twisted rudder parameters, and $\$length\$$, $\$thick\$$, $\$x\_pos\$$ for the bulb parameters. The script opens a `.ffw` temporal file containing the design project, then all parameters chosen by the optimizer algorithm are changed and new geometry is created for further meshing and simulation.

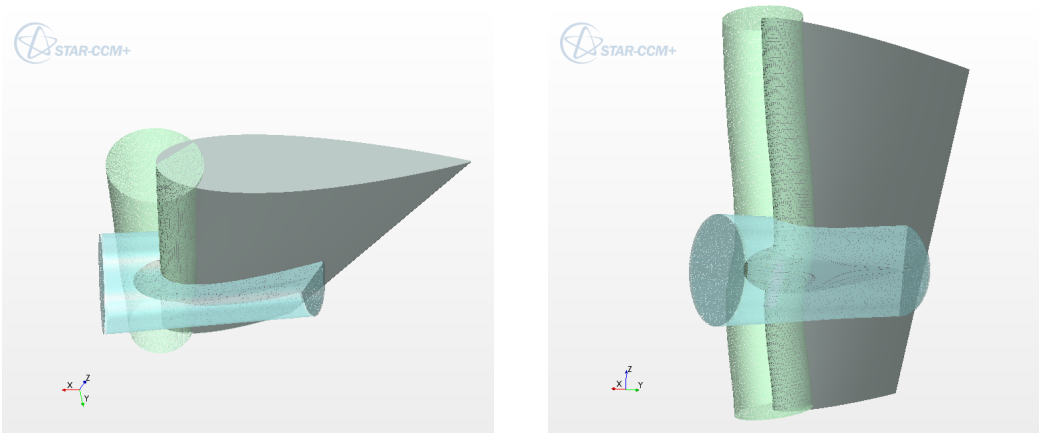

Figure 3.6.: Parametric cylinder for leading edge and bulb refinement

3.3. Data Collection and Analysis

In order to analyse the simulations, several tools can be used. The first graph to monitor convergence is the resulting forces on the hull per iteration, shown in section 2.4.2. Moreover the most important graph for this work is the resulting forces on the rudder, for this reason a new command in the script plots the forces and moments acting only on the rudder.

As results are registered in a folder for every coupling step, the data needs to be processed (eliminate brackets) and appended together in a unique file. The Python script `forces_cor.py` searches for the forces files (either for rudder or total), created by the simulation (functions in control dictionary). After getting all forces data in a unique file ("forces.dat" or "forces_rudder.dat"), the script `plot_forces.pl` is called and results are plotted.

To get a unique value for every result of interest in order to be analysed in FS-Optimizer, the desired results history data are averaged over the last 100 iterations. To get these results the script used is `collectProcalOutput.py`.

Results are taken both from Procal and Foam post-processing folders, then appended to a file called "results.txt". This file contains the results for lateral and axial forces from the OpenFoam simulation (Fy_{rudder}, Fy_{total},R_{rudder} and R_{total}), also thrust, revolutions and torque from the Procal simulation (T, n and m_x), as well as a calculation of the propeller load (Advance ratio J).

Regarding further post-processing analyses like wake study or flow visualization, it is done using the tool *paraview*. An automatic routine for images generation of several designs is `plots.py`, which looks for the latest time step results in the OpenFoam folder, opens *paraview* in a predefined state and saves the necessary images (velocities, streamlines, contours, etc) for a handy visual comparison.

```
openProject("tmp.ffw")

// ------------------------------------------------------------------
// DESIGN VARIABLES
// ------------------------------------------------------------------


// twist angle
|01_functions|twist_angle|auxiliary|angle_bottom.setValue($ang_b$)
|01_functions|twist_angle|auxiliary|angle_top.setValue($ang_t$)
// rotation axis
|01_functions|rotation_axis|auxiliary|rotation_axis.setValue(
   $x_axis$)
// bulb
|02_parameters_bulb|Length_bulb.setValue($length$)
|02_parameters_bulb|Thickness_bulb.setValue($thick$)
|02_parameters_bulb|XposBulb.setValue($x_pos$)


// ------------------------------------------------------------------
// DESIGN VARIABLES END
// ------------------------------------------------------------------


// export the new variant
|Box01.exportSTARCCMSTL("box.stl")
|Bulb01.exportSTARCCMSTL("bulb.stl")
|bulbcil.exportSTARCCMSTL("bulbcil.stl")
|cilinder01.exportSTARCCMSTL("cilinder.stl")
|Rudder01.exportSTARCCMSTL("rudder.stl")

// close FFW
exit(true)
```

Figure 3.7.: CAESES geometry (.stl files) generation script

4. Mesh Generation

A mesh analysis is necessary in order to get an appropriate mesh that solves the problem with a reasonable accuracy but in the same way with the lowest computational time as possible. This is a very crucial step in the optimization procedure, since several geometries are to be analysed and each simulation would take a tremendous amount of time to converge if the mesh is too refined, but at the same time accuracy suffers if the grid is too coarse.

In this work two different studies are presented: one for the coupled method and another for the *RANS* simulation (this is propulsion and resistance study). Results are compared to the DTC SVA test [11], although the present design has a twist angle of -11.65° at the top and 9.18° bottom. Since the twist is not the same as the rudder used by the SVA test [11] (-5° and 5°), there is a new intrinsic error on the results when comparing to those obtained experimentally on the SVA test, which is not taken into account.

Table 4.1.: Geometrical and environmental data for the *DTC* [11]

		Full scale	Model scale	
Hull				
Scale factor	λ	59.407		[-]
Length between perpendiculars	L_{pp}	355.0	5.976	[m]
Beam	B	51.0	0.859	[m]
Mean draft	T_M	14.5	0.244	[m]
Static trim	ϑ	0	0	[deg]
Block coefficient	C_B	0.661	0.661	[-]
Wetted surface area	S_w	22032.0	6.243	[m^2]
Ship velocity	v_s	25 kn	1.6686 m/s	
Propeller				
Number of blades	N_{blades}	5		[-]
Propeller diameter	D_p	8.911	0.150	[m]
Pitch ratio	$P_{0.7}/D_p$	0.959	0.959	[-]
Area ratio	A_e/A_0	0.800	0.800	[-]
Chord length at $r/R_p = 0.7$	$c_{0.7}$	3.208	0.054	[m]
Propeller skew	θ_{eff}	31.97	31.97	[deg]
Environment				
Water density	ρ	998.4		[kg/m^3]
Kinematic viscosity	ν	$1.090 \cdot 10^{-6}$		[m^2/s]

The Duisburg Test Case (DTC) hull is a typical 14,000 TEU container ship design with a twisted rudder and a Costa Bulb. It was developed as a validation test case at the Institute of Ship Technology, Ocean Engineering and Transport Systems at the University of Duisburg-Essen. The geometry as IGES file was manually converted for the use with the Star-CCM+ mesher. Geometrical and environmental parameters used in the coupled simulation are listed in Table 4.1.

The first step for a rudder mesh study is the creation of a parametric geometry (section 3.2), then the mesh is set up based on criteria described in section 4.1 and finally a refinement is achieved on the most critical areas in order to avoid numerical fluctuations or divergence in the results. Finally every mesh is tested using the method (either coupled or uncoupled in section 4.2) and results are analysed (section 4.3) for a final mesh selection.

4.1. Meshing procedure

The meshing procedure is well described by Herbel [6]. All grids used are generated with the Star-CCM+ mesher in batch mode. To be used with OpenFOAM the meshes are exported from Star-CCM+ in `.ccm` format and converted using the `ccm26ToFoam` utility.

Each refinement is performed by splitting cells uniformly in all directions. Base size is obtained by dividing the reference length by a number of cells per reference length ($RefCells$ in this work), which can be used to control the global mesh resolution. A first mesh refinement was created based on this procedure (mesh *RefC16* in Figure 4.2), but due to complexity of the geometry and sharp edges, several faces with error appeared surrounding the hull and rudder surfaces.

To measure the suitability of the mesh, different quality criteria are defined based on geometrical properties and on simulation results, carried out with same meshes. This is also well explained by Herbel [6]. In addition, the distribution of the non-dimensional wall-distance of the first grid point y^+ is evaluated as a measure for the boundary layer resolution, for which values below 5 and above 30 (Buffer sub-layer) limit the accuracy of the applied turbulence models and should be avoided according to Andersson et al.[1], although in the coupled method, the turbulence uses an *all* y^+ wall treatment.

The evaluation of meshes is conducted using mesh quality statistics that are created with tools provided by Star-CCM+ and OpenFOAM. Some properties for measuring mesh quality on the generated output are: orthogonality, concavity, aspect ratio, skewness, cell volume ratio, face area, face validity and cell quality.

One of the main sources of error found in the initial mesh *RefC16* was the so-called non-orthogonality on faces (in consequence the mesh is not used), which is shown in Figure 4.2 with red faces as problematic. Higher than 85° non-orthogonality might lead

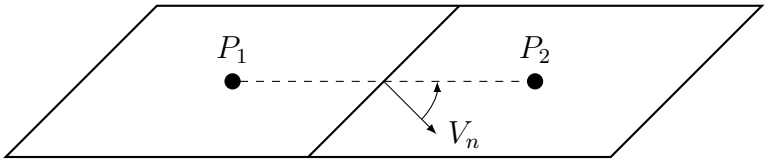

Figure 4.1.: Orthogonality Definition in 2-D [6]

to inaccuracies or solver instability, as Herbel indicates [6]. To achieve maximum accuracy for the approximation of the diffusive flux, the imaginary line connecting the centers P_1 and P_2 (in Figure 4.1) of two adjacent cells should be orthogonal to their common cell face. The angle between this line and the face normal vector V_n is the non-orthogonality angle (zero for optimum accuracy).

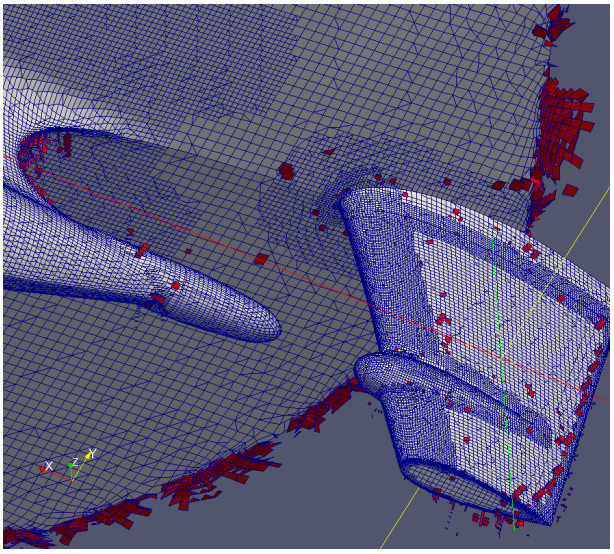

Figure 4.2.: Non orthogonal faces in initial mesh (RefC16)

For meshes studied in this work a refinement on the leading edge of the rudder and surrounding the bulb was achieved by the creation of a parametric cylinders shown before, these refinements are isotropic, about 40% of base size. Some other important refinements are done along the sharp edges and corners, such as rudder edges. These refinements are obtained by fraction of base size as well.

To set up a series for the mesh study, a case table presented in Figure 4.2 was created to specify the respective case names and the according variation on specific parameters such as: number of reference cells, concavity limit, convex limit and grid offsets.

Case table (Table 4.2) shows that after changing the values for `ConcaveLim` and `ConvexLim` in the initial mesh (*RefC16*) into a coarser mesh (*Coarse 12*), all the subsequent grids have the same values, because non-orthogonality is reduced using these parameters. Finally, an Offset was assessed to some meshes (meshes with 16 and 22 $RefCells$) in order to prevent very high skewness on overlapping (or close to each other) cells. Different meshes are presented in Figure 4.3 (coarsest to finest). Mesh Fine 24 is not studied, because it

Table 4.2.: Content of the caseTable.csv file for the mesh study

Name	RefCells	ConcaveLim	ConvexLim	GridOffsetX	GridOffsetY
RefC16	16	120.0	275.0	0	0
coarse	12	50	220	0	0
fine16	16	50	220	0	0
fine16n	16	50	220	0.31	0.35
fine20	20	50	220	0	0
fine22	22	50	220	0.41	0.32
fine22n	22	50	220	0.41	0.32
fine24	24	50	220	0.41	0.32

includes a high quantity of cells (about 12 million), therefore the simulations would need a tremendous amount of computational time.

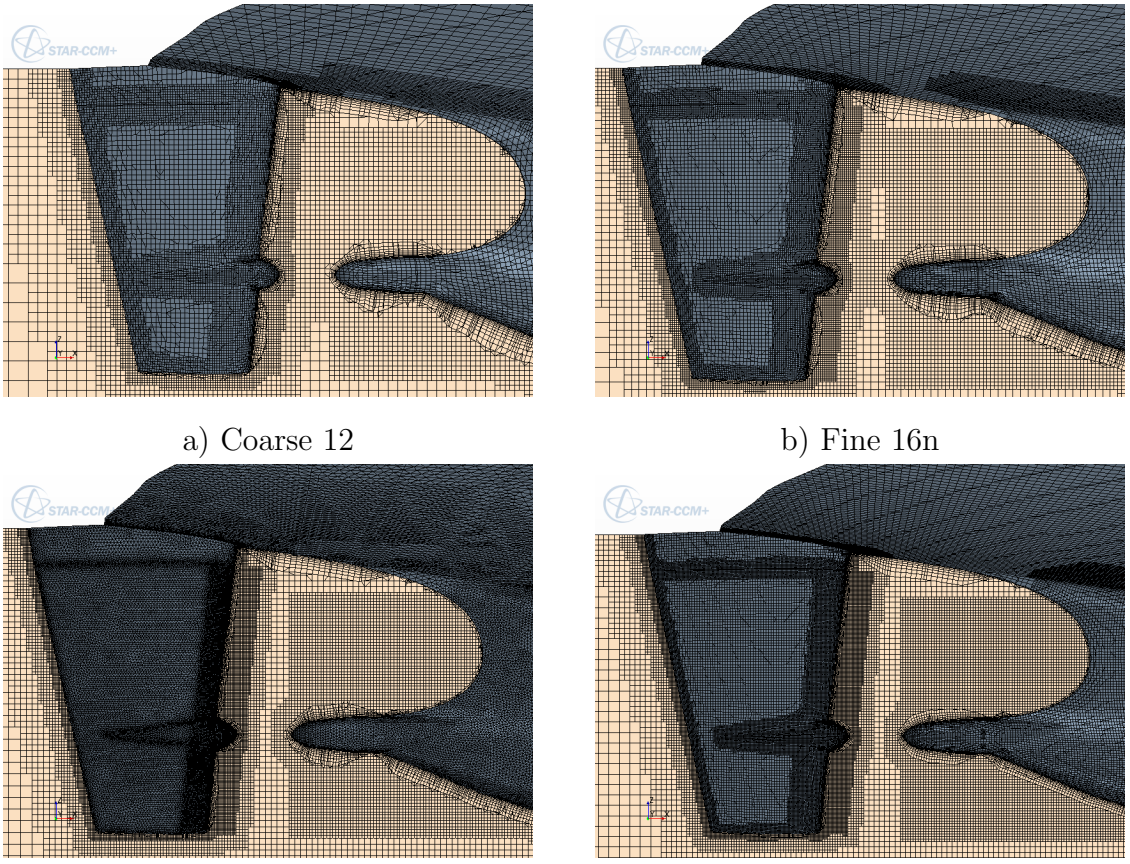

a) Coarse 12 b) Fine 16n

c) Fine 20 d) Fine 22

Figure 4.3.: Generated Meshes

4.2. Set up of Coupling Scheme

In this chapter the Set up of the Coupling Scheme is explained according to Schenke's coupled method manual [15]. Since the mesh used in the Potential flow simulation is radial, it does not correspond to the OpenFoam mesh, thus the first step before executing the simulation is the mesh coupling (see also section 2.4.1). Then definition of parameters in the input folders is configured, for the specific case, shown in Table 4.3. Once this is defined, the project is ready to compile and run.

Table 4.3.: Parameters controlling the coupled simulation [14]

Propeller representation	Interpolation of the force field: Transfer of the force field: Coordinates:	N_n, N_m R_S, std C_{30}, x_{p3}
Wake disc	Size: Distance: follow leading edges:	f_{root}, f_{tip} x_{w0} true/ false
Coupling	Number of coupling steps: Coupling steps convergence:	n_{steps} n_{hist}, n_{cos}

In Table 4.3, N_n and N_m indicate the number of collocation points in circumferential and radial direction (for force interpolation, $N_n = 120$ and $N_m = 50$ in this case). Parameter R_S specifies the radius of the transfer sphere that captures the *RANS* cells which each propeller panel force is distributed to (see Figures 2.7 and 4.4), in this work $R_S = 0.01$. According to the method, it turned out to be good practice to set $std = R_S/2$, such that the sphere captures a range of two standard deviations. C_{30} is the transformation matrix that enables for vector transformation between propeller reference system 0 and RANS reference system 3, x_{p3} denotes the origin of propeller disc with respect to system 3 (defined by Schenke [14]).

f_{root} and f_{tip} are factors for increasing the inner or outer radius of the wake disk (with respect to hub and propeller radius respectively), thus intersection between wake disc and hull is avoided. In this work $f_{\text{root}} = 1.6$ and $f_{\text{tip}} = 1.2$. x_{w0} is the distance of the wake disc from the propeller plane, positive upstream. User might define as well whether the wake disk shall be plain or cambered following the surface swept by the blade's leading edges.

As it was explained in section 2.4.2, the convergence behaviour depends both in the number of iteration steps to take into account the inclination of the best fit line in the error residuals (n_{hist}) and changes of sign encountered by the inclination (n_{cos}). In this work it is set to $n_{\text{hist}} = 100$ and $n_{\text{cos}} = 4$. The overall number coupling steps is defined as $n_{\text{steps}} = 7$.

In Figure 4.4 some of the parameters are shown. Top figure (a) depicts an example of propeller cell set generated by `topoSet`. Figure (b) shows the polar grid containing the stationary propeller forces, obtained by tracing the propeller blade panel forces for the duration of one propeller revolution, this is controlled by number of collocation points N_n and N_m for the propeller disc. Figure (c) shows the relation of outer and inner disc radius adjusted to the propeller.

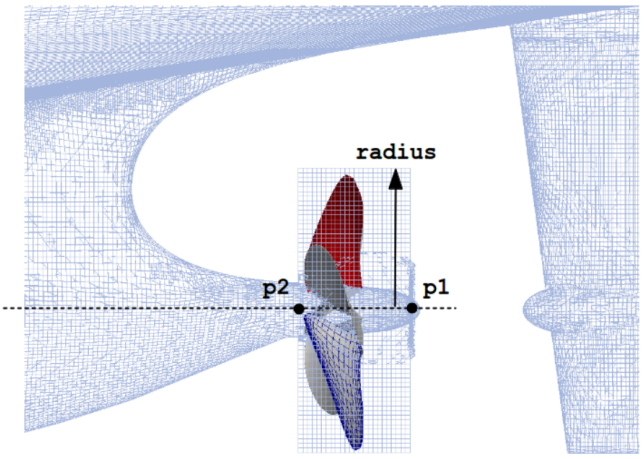

a) Propeller cell set

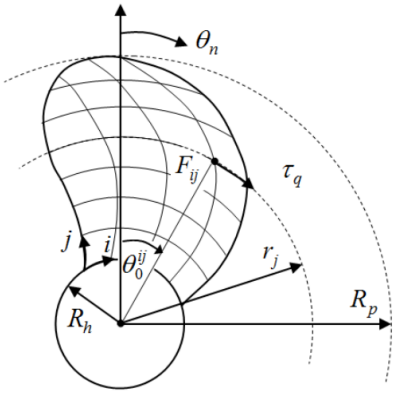

b) Schematic of the stationary propeller disc (polar grid, right) derived from the trace of the panel forces

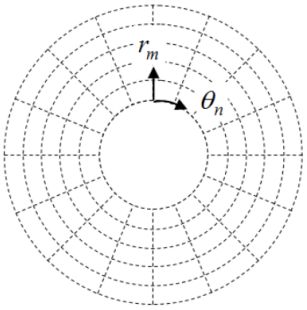

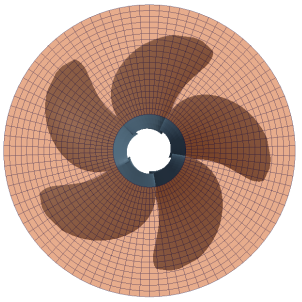

c) Inner and outer disk radius adjustment

Figure 4.4.: Propeller cell set and Wake disk radius adjustment [15]

Lastly after the convergence is achieved, the routine for result collection and analysis is run (see section 3.3). These scripts were partly designed during the development of this master thesis in order to ease or improve the collection procedure defined initially by Schenke [14].

4.3. Mesh Convergence

The mesh analysis is based on a 2% criterion, meaning that when a grid refinement reaches a relative error equal or less than 2% (compared to the consequent mesh), mesh independence is achieved.

Automatic mesh and set up generation procedure adopted in this work was developed by Herbel [6], it was as well used to set up and run simulations for a double-body resistance test with OpenFOAM (resistance study without coupling method). All fluid and input parameters were specified according to the values provided in the model test reports used as reference (cited in Table 4.1).

Reference data was evaluated experimentally at the *Potsdam Model Basin* (SVA) [11]. The available report includes resistance, propulsion and roll-decay values. Required free surface resistance values are taken from model test report shown in table 4.4.

Table 4.4.: Experimental resistance coefficients for the DTC hull [11]

Resistance study			
Velocity	V	1.668	[m/s]
Froude Number	F_R	0.2140	[-]
Resistance	R_T	31.83	[N]
Total resistance coefficient	$C_T[10^3]$	3.626	[-]
Reynolds Number	$Re[10^{-6}]$	9.5	[-]
Friction resistance coefficient	$C_F[10^3]$	3.0291	[-]
Residual resistance coefficient	$C_R[10^3]$	0.5967	[-]
Propulsion study			
Thrust deduction fraction	t	0.090	[-]
Friction deduction	F_D	13.947	[N]

In section 4.3.1 the coupled method was tested for the propulsion study and results for different meshes are studied. Then in section 4.3.2 a resistance study is performed, it means without the influence of the propeller (non-coupled $RANS$ method), in order to calculate the free surface resistance (with data from SVA report [11]).

4.3.1. Propulsion study - Coupled Scheme

This study was performed to the four selected meshes (presented in Figure 4.3). Results obtained are summarized in Table 4.5 and diagram in Figure 4.5 shows resistance and rudder forces for each mesh. These values do not present significant sensitivity to mesh refinement, for instance mesh convergence is accurate with a maximum deviation of 0.16% between mesh Fine16-n and Fine20 in the C_TFOAM. This means that the mesh is accurate enough to calculate overall ship forces with a refinement of 16 $RefCells$.

Table 4.5.: Propulsion mesh study for the DTC hull

$RefCells$	No. cells[10^6]	T [N]	R_{Total} [N]	C_T FOAM	R_{rudder} [N]	Fy_{rudder} [N]
12	3.272	17.25	29.958	$3.4525 \cdot 10^{-3}$	0.5878	-0.2379
16-n	5.390	17.36	30.005	$3.4579 \cdot 10^{-3}$	0.6159	-0.2912
20	8.180	17.33	30.055	$3.4637 \cdot 10^{-3}$	0.5839	-0.2079
22	9.635	17.32	30.045	$3.4625 \cdot 10^{-3}$	0.6038	-0.0111

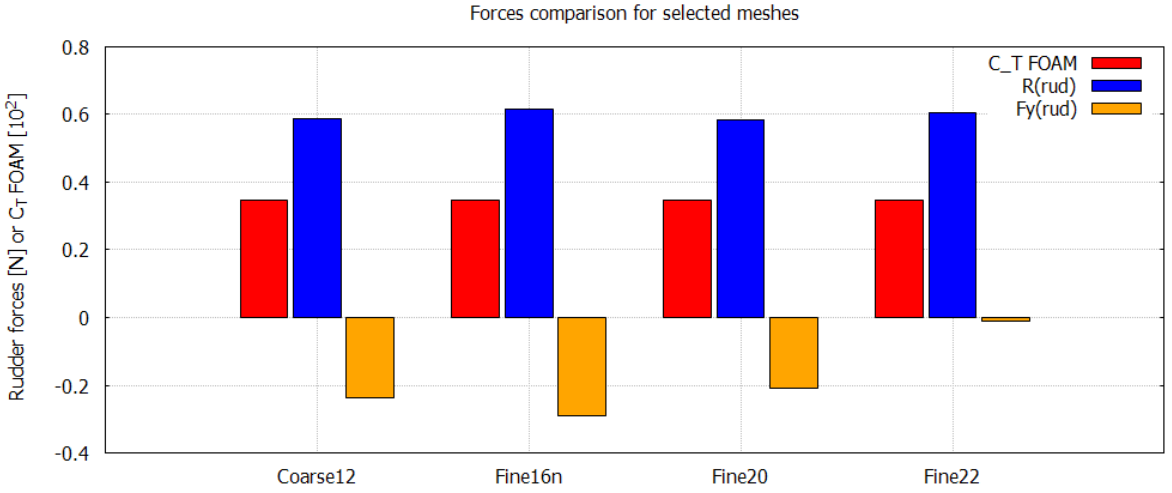

Figure 4.5.: Forces comparison for the DTC coupled mesh study

Furthermore, when looking closely to rudder forces (blue and yellow in Figure 4.5), it is noticed a low sensitivity to mesh refinement for the longitudinal force (R_{rudder}) because the rudder is at zero degrees of incidence. This sensitivity is of the order of 2% between mesh Fine16-n and Fine22. However the lateral force (Fy_{rudder}) is highly affected with the mesh resolution and this can be due to diverse reasons. For example, even for a coarse mesh with $RefCells$ 16, lateral pressure force converges in an oscillatory trend. This could be a topic for further studies (see Figure 4.6).

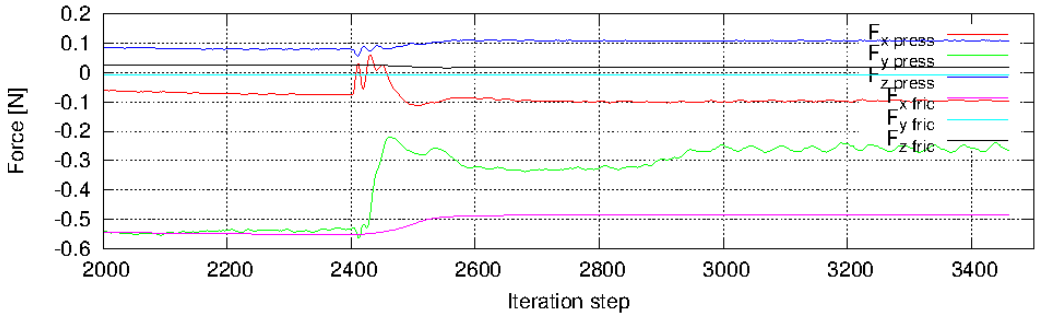

Figure 4.6.: Rudder forces convergence for Mesh Fine 16

This lift force increases in a steep rate when the mesh refinement also increases, this could be due to some mathematical uncertainties or fluctuations along the sharp edges of the

rudder (bottom leading edge). In order to verify this hypothesis, an additional analysis was performed in mesh Fine22-n (which has a low refinement around the rudders' bottom leading edge), comparing the evolution of pressure distribution along sharp edges with initial mesh Fine22.

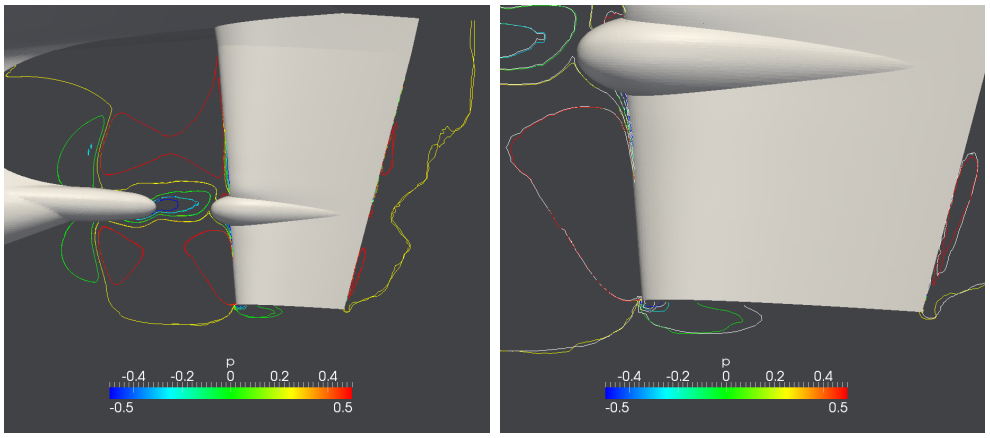

Figure 4.7.: Pressure contour around the Rudder's bottom

The case in Figure 4.7 shows the pressure contours around the rudder and propeller hub. Here in the left graph there is a slight difference specially on bottom leading edge pressure, which could cause a difference in lateral force. Right graph is a close-up of this problematic zone, and notice that low pressure zone for mesh Fine22-new (white contours) is bigger than in mesh Fine22 (coloured contours).

It is decided that lateral force on the rudder is not further taken into account, thus results and optimization rely only on total and rudder resistance from OpenFOAM results, as well as torque, thrust and revolutions from Procal results. For this purpose, it is considered that mesh Fine16-n is accurate enough to do the up coming studies.

4.3.2. Resistance study - RANS Simulation

This study was performed to the most refined meshes (Fine20, 22, 22-new and 24) since the coarser meshes were in a non reliable range for the coupled simulation in the very beginning (as shown in section 4.3.1), although after the modification to mesh Fine16 the convergence was present in the new resulting mesh. Results obtained are summarized in Table 4.6 and diagram in Figure 4.8 shows the computed double body resistance values for this mesh study.

The computed resistance values do not show a significant sensitivity to the mesh resolution, giving a difference of around 0.64% between mesh Fine22 and Fine24. At this point it could be defined that the mesh resolution is sufficiently high with $RefCells = 22$ (without modification), but the resulting mesh is not used for further examinations since

Table 4.6.: Resistance mesh study for the DTC hull

$RefCells$	No.cells[10^{-6}]	C_T Exp	C_F ITTC '57	R_{Total} [N]	C_T FOAM
20	8.180			27.867	$3.211 \cdot 10^{-3}$
22	9.635			27.814	$3.205 \cdot 10^{-3}$
22-n	9.540	$3.626 \cdot 10^{-3}$	$3.0291 \cdot 10^{-3}$	27.819	$3.206 \cdot 10^{-3}$
24	11.717			27.793	$3.203 \cdot 10^{-3}$

the quantity of cells enlarge the computational time, thus as mentioned before grid Fine16-n is used.

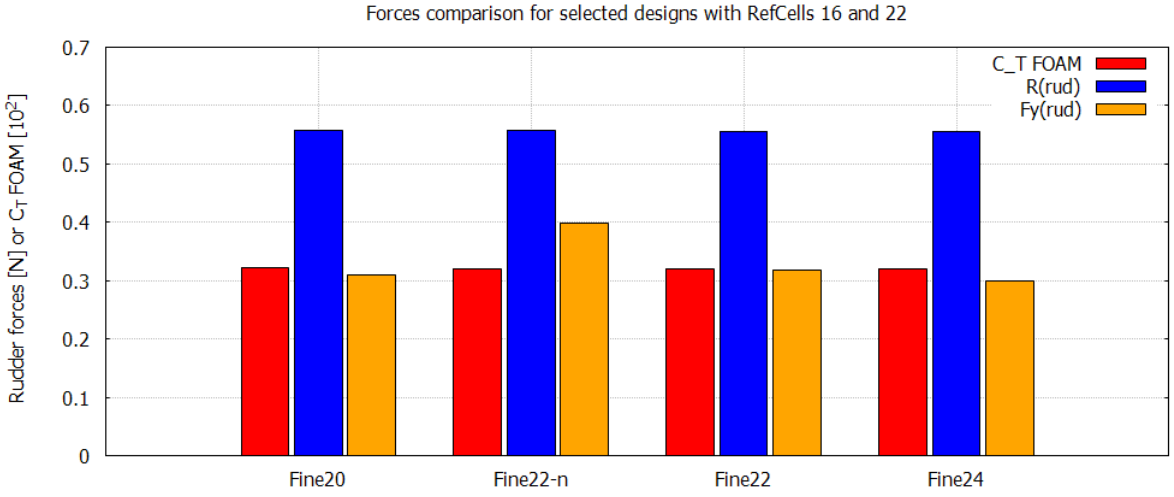

Figure 4.8.: Forces comparison for the DTC Double-body resistance mesh study

Moreover, all meshes show a low sensitivity for mesh resolution on the rudder resistance as expected, about 0.45% difference between mesh Fine20 and Fine24. The lateral force however is a little more sensible to the mesh refinement (as for coupled method) with 3% difference. A peak is noticeable on the modified Fine22-n mesh, this means that the modification is not at all reliable in this case.

This study presents better grid independence because the propeller stream is not affecting the rudder, therefore all the forces on the rudder should converge faster. However in Figure 4.9 the convergence of rudder forces is shown for mesh Fine 22 showing the last 1500 iteration steps of the simulation. It is more clear with this image how the lift generated by the rudder can not be a very accurate result to study, because it has not find a convergence after 2600 iterations.

Figure 4.10 shows a visualization of the y^+ distribution on the aft-ship. As mentioned in Section 4.1, values between 5 and 30 should be avoided, even though an $all-y^+$ treatment is used. It is recognizable that the wall distance is in a favourable value range over the hull surface with the exception of the rudder leading edge and hull bottom.

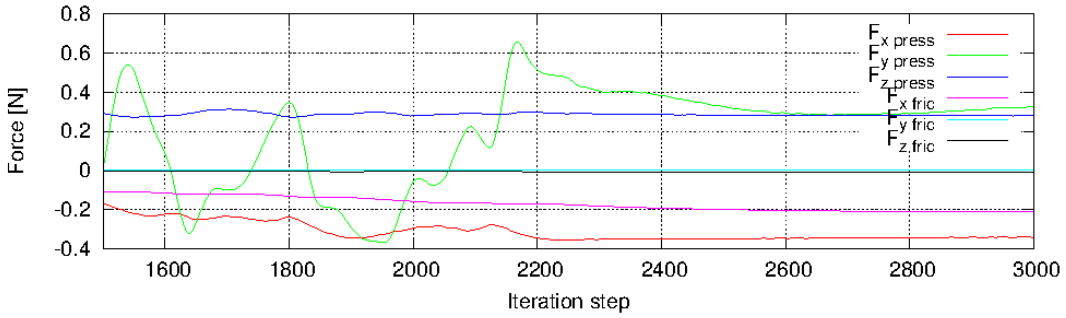

Figure 4.9.: Rudder forces convergence for Mesh Fine 22 uncoupled

The calculation of y^+ in this case was done for the non-coupled scheme, meaning that the propeller slipstream is not considered, in consequence the flow over the rudder is influenced only by the ship speed and hull presence. On the other hand (in the coupled method simulations) since the flow behind the propeller is accelerated, the y^+ values on the rudder surface are assumed high enough to not to fall in the aforementioned avoidable region. It is important to notice that the meshing procedure is based on Herbels' [6] studies. This means that experience with this type of mesh shows a good behaviour when working with $all - y^+$ wall treatment.

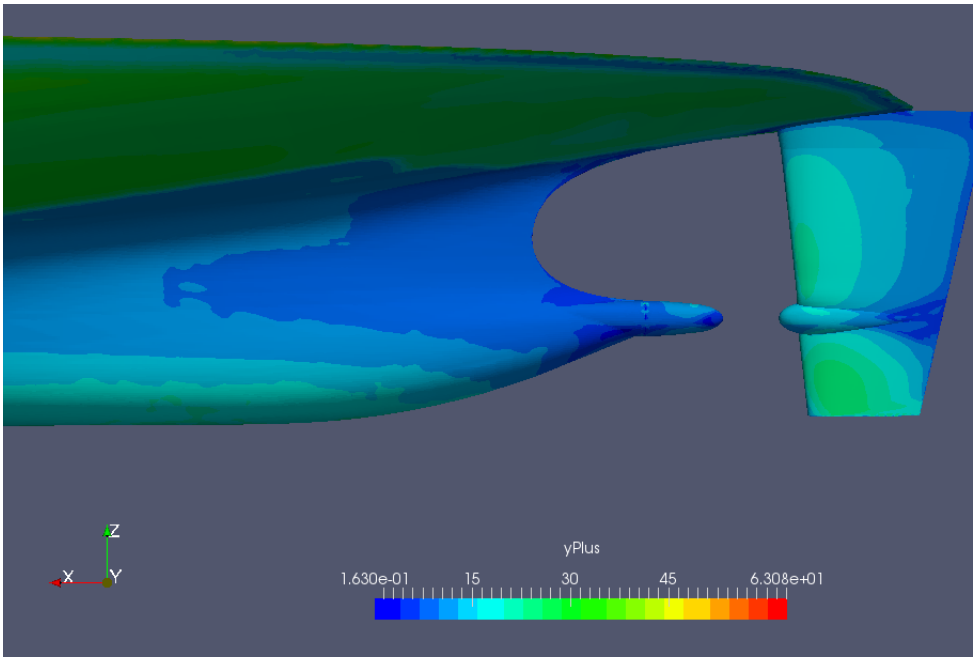

Figure 4.10.: y^+ distribution on the aft-ship computed with OpenFOAM

5. Initial Rudder: case without twist

An initial rudder geometry without twist is studied in order to have a starting point and compare the optimization design. The influence of the bulb is studied in this chapter. The bulb is the same used in the optimization procedure and its shape is optimized in Section 6.3.

In order to simulate this design (and further optimization runs), an operating point routine created by Schenke [15] is applied (Section 5.1) and then results for the initial rudder are presented (Section 5.2).

5.1. Operating point

This methodology is pointed out both from Schenke [14] and Herbel [6]. The self propulsion point for a specific hull-propeller combination is defined as the rotation rate n required to generate the thrust needed to overcome the resistance R_{Tp} at a given ship speed. In self propulsion model tests the difference of the skin friction coefficients between model and full scale ships is commonly accounted for by the application of an external force F_D.

In the coupled simulations of the model carried out in the scope of this thesis, the self propulsion point is evaluated for a given ship speed as the propeller rotation rate, where:

$$T = R_{OF} + R_{FS} - F_D \tag{5.1}$$

Since no free surface resistance simulations were carried out, the friction deduction F_D for the calculation of R_{Tp} was taken from the model SVA test report in [11]. R_{FS} was evaluated from a double body resistance simulation carried out for the DTC hull with the rudder from the mesh study simulations, using Herbel's automatic procedure and the experimental R_T.

When considering the respective sign, R_{Tp} and T can be added to obtain the resistance residual R_{Res}. Table 5.1 shows the calculated R_{Res} values for the two propeller rotation rates that have been used as input for the simulations. The self propulsion point was interpolated from these values as rotation rate n_{OP} at which $R_{Res} = 0$ (see Figure 5.1).

Table 5.1.: DTC Operational point results

$n[s^{-1}]$	$R_{Tp}[N]$	$R_{FS}[N]$	$F_D[N]$	$T[N]$	$R_{Res}[N]$
12.332	-30.486	4.016	13.947	17.32	-2.19032
13.36	-30.045	4.016	13.947	22.3	2.30808
				$\mathbf{n}_{OP}[s^{-1}]$	12.945

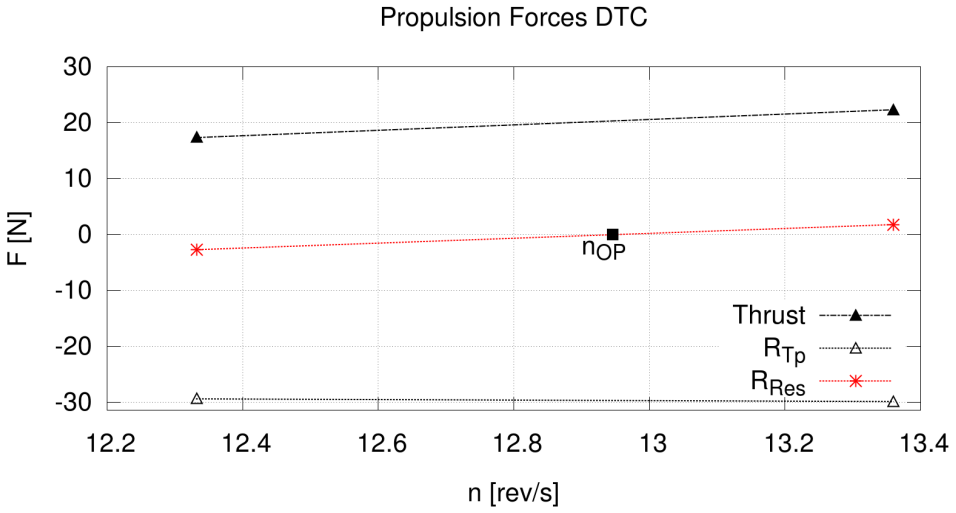

Figure 5.1.: Determination of the operating point

Schenke [15] presents a methodology to control the propeller revolutions in order to get the operating point while running the coupled simulation by means of a simple P-controller. It adjusts the propeller's rotational rate such that an equilibrium between propeller thrust and ship resistance is achieved.

Under the assumption that the current rotational rate n_i is proportional to the difference $\Delta F_i = R_i$-T_i between the current propeller thrust T_i and the current ship resistance R_i, the new rotational speed is obtained as:

$$n_{i+1} = n_i + \frac{\Delta F_i}{R_i} n_i = \left(2 - \frac{T_i}{R_i}\right) n_i \tag{5.2}$$

Applying relaxation by λ yields:

$$n_{i+1} = \lambda \left(2 - \frac{T_i}{R_i}\right) n_i + (1 - \lambda) n_i \tag{5.3}$$

A body force model has been implemented for double body simulations only. In this case R_i (for instance R_{Tp}) is composed of the double body resistance obtained by a RANS solver and an additional free surface component obtained by the aid of experimental data minus friction deduction (see Equation 2.13).

The relaxation factor $\lambda = 1$ means that no relaxation is applied and $\lambda = 0$ means that the current rotational rate is not changed at all. According to Schenke [15] it is not recommendable to start with the control at the very first coupling step, since at this point the combined hull and rudder forces are not sufficiently converged yet. For this reason in the optimization procedure, the number of coupling steps is increased to 12.

Figure 5.2 depict the convergence of rotational rate, thrust and resistance for an initial rotational rate being smaller than the operating point. Schenke [15]recommends to set the initial rotational rate smaller, but such that the propeller still generates positive thrust at the initial open water simulation.

This recommendation is based on the fact that PROCAL is prone to numerical instability for negative angles of attack. By setting the initial rotational rate too small, the initial control step (which is supposed to take more computational time), increases the rotational rate and thereby reduces the risk of ending up in negative thrust.

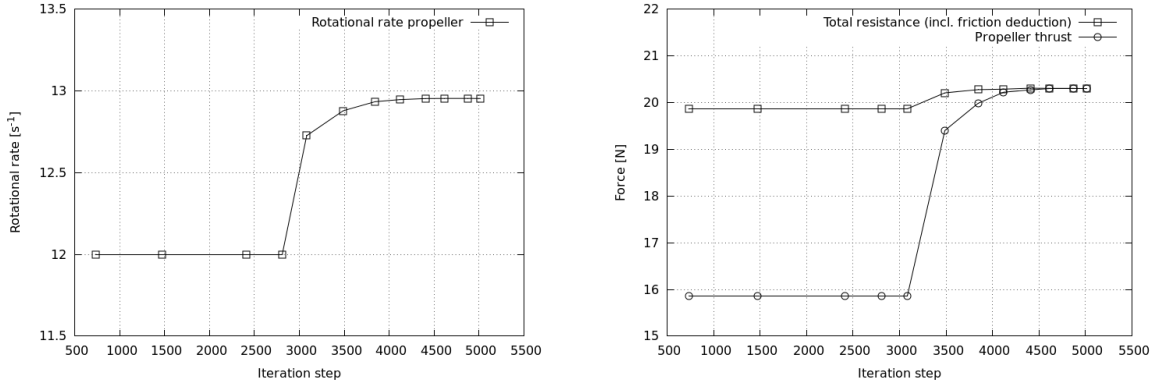

a)Rotational rate approaching the operating point

b)Thrust and resistance approaching the operating point

Figure 5.2.: Control of revolutions example

5.2. Results non-twisted Rudder

Table 5.2 presents the averaged results for an initial Rudder without twist, both with and without Costa bulb. The first value calculated is the advance coefficient (J), which has very slight differences from a plain rudder to a rudder using a bulb, this is noticeable since the propeller wake is nearly the same, thus the rotational rate of the propeller does not vary significantly at the operating point.

Table 5.2.: Results for initial Non-twisted Rudder

Result		Rudder alone	Rudder+Bulb	% delta
J		0.6111	0.6109	0.033
n	[rev/s]	13.44	13.47	0.22
m_x	[Nm]	0.515	0.516	0.14
T	[N]	21.05	21.07	0.095
R_{total}	[N]	30.42	30.44	0.055
R_{Rudder}	[N]	0.61	0.65	5.26
Fy_{total}	[N]	−1.05	−0.82	27.41
Fy_{Rudder}	[N]	−0.72	−0.44	64.70
P_D	[W]	43.52	43.68	0.36
η_D		0.807	0.804	0.28

In this case, the total resistance of the ship (the OpenFoam result R_{total}) is essentially not changed, but the rudder resistance itself R_{Rudder} is increased by 5.257%, because of the bulb higher thickness. Moreover the bulb is intended to reduce the hub vortex generated in the propeller slipstream, thus an increase in thickness in this zone is recommended even if the resistance is increased.

On the other hand, it is seen that the propulsion efficiency (η_D) is decreased by 0.28% (due the increase of torque m_x) when using this specific bulb, therefore augmenting the delivered power (P_D). It is important to note that this bulb was not designed following any rules or guidelines, since it is subjected to an optimization procedure in the following chapter.

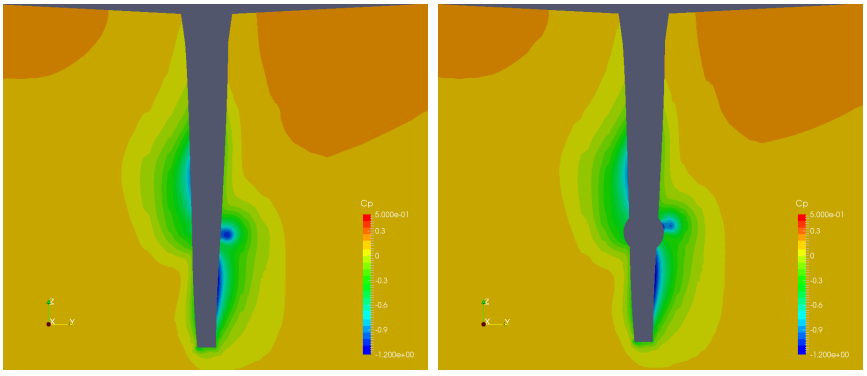

a) Rudder without bulb b) Rudder with bulb

Figure 5.3.: Pressure coefficient contours at $X = 0.03$

In Figure 5.3 the gray zone is the transverse view at rudder leading edge (LE). The blue circle at the right of the rudder is the so called hub vortex. It is seen that the bulb influences the pressure distribution around the rudder, but more specifically redirects the rotational flow coming from the propeller, reducing the hub vortex magnitude. This in consequence affects the lateral forces and cavitation risk.

It is seen this effect in Figure 5.4, where the axial velocity contours at the trailing edge (TE) of the rudder are presented. It is seen that negative axial velocities are reduced (blue zones) because the bulb tends to align the flow with its own axis. At the LE it is expected that the flow is mainly affected by the propeller stream, thus the variations are not very high for the same rudder design only with bulb presence.

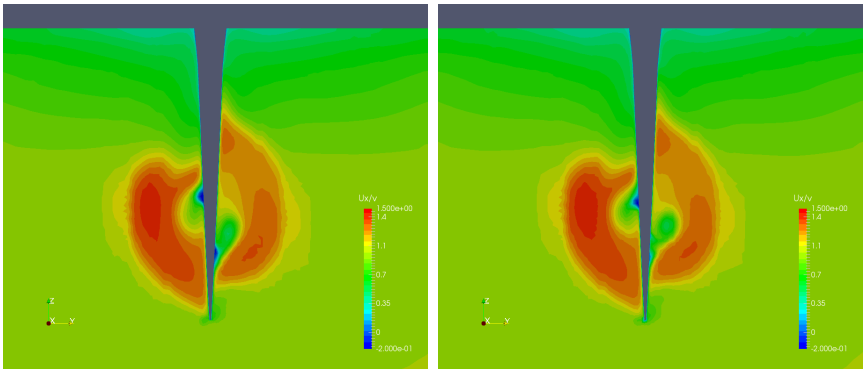

a) Rudder without bulb b) Rudder with bulb

Figure 5.4.: Axial velocity contours at $X = -0.05$

Regarding lateral forces - Lift (both Fy_{total} and Fy_{Rudder}), there is a high variation on this value, although it is still pointing in the same direction (towards Starboard), therefore the lift should be subjected to further analyses.

The purpose of the optimization is to reduce the drag and lift generated by the rudder, but there is a high probability that the lateral force is generated mainly due to noise or fluctuations in the calculations since the order of magnitude of this result is very small compared to the total axial forces and a slight variation on pressure over the surface affects it significantly (as mentioned before in Chapter 4.3.1). From this point, the lift is not considered as a minimization objective for the FS-Optimizer but as a monitor value.

Finally in Figure 5.5 a representation of the rudder (starboard and port views) is shown with the pressure distribution and streamlines that illustrate what has been mentioned in this chapter.

The baseline design for the optimization procedure is therefore the non-twisted rudder with bulb, although the bulb in this case is not well designed. As it is noticeable, the presence of a bulb changes the behaviour of the flow, especially the hub vortex. This means that the pressure distribution over the rudder surface varies, therefore the forces change as well. This is appreciable looking at the pressure coefficient in Figure 5.5, in which the blue zones are diminished using a bulb. This is an effect of reducing the hub vortex.

These results are taken as starting point for the further optimization procedure. In Chapter 6 the effects of reducing the hub vortex and flow alignment are discussed in detail.

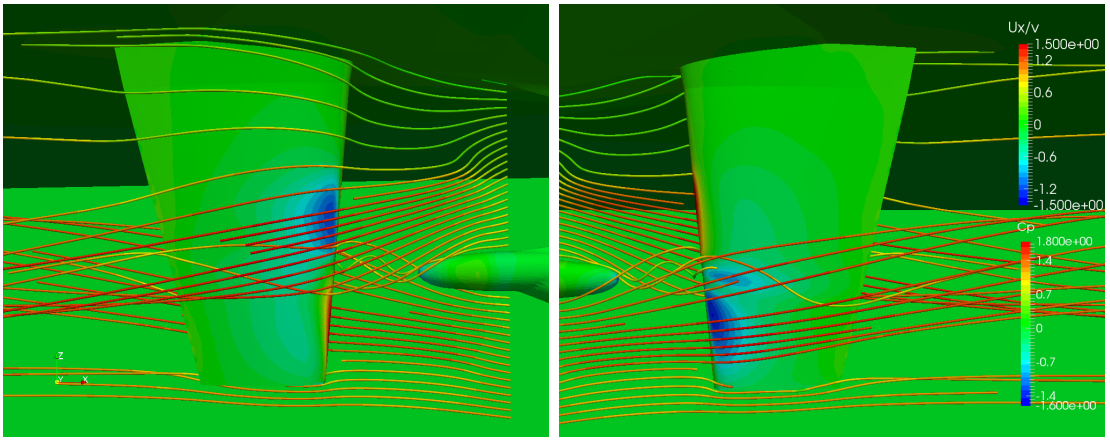

a) Rudder without bulb

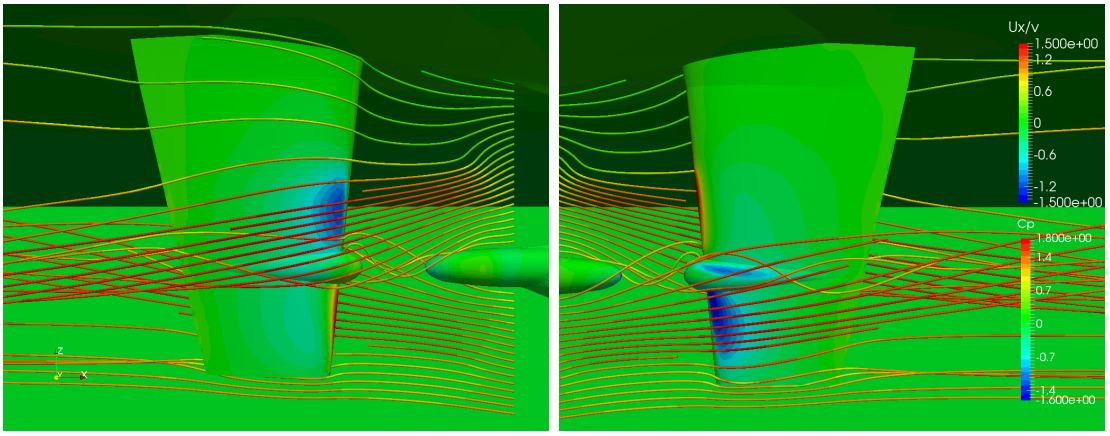

b) Rudder with bulb

Figure 5.5.: Initial rudder pressure distribution and streamlines

6. Optimization

This Chapter presents the final results for different optimization studies. A first study (Section 6.1) corresponds to the optimization test using an initial Sobol followed by a NSGA-II based algorithm, based on these results a new grid study is presented in order to confirm the initial Mesh selection from Chapter 4. The second study (Section 6.2) presents the results for an optimization procedure using a NSGA-II based algorithm with a corrected objective and geometry. Finally study 3 (Section 6.3) shows the results for a bulb optimization with a fixed twisted rudder selected from results in study 2.

For all studies, variables are selected from the rudder geometry, as it is designed to change twist angle and axis, as well as bulb thickness, length and longitudinal position. For further optimization research, other variables might be taken into account as: rudder taper, chord and height.

Rudder parameters vary according to the design criteria. Variation goes from -15° to 15° for the offset points in the twist angle (defined as ang_1 for the top, ang_2 for the bottom). Rotation axis varies from 0.2 to 0.4 (defined as x_axis). Bulb parameters vary from 0.2 to 0.4 for thickness, 6.5 m to 9 m for length and 0.1 m to 2 m for bulb longitudinal position (in front of rudder) (values in real scale). These are defined as $ThicknessB$, $LengthB$ and $XposB$.

The limits on the variable domains are included in their definition and no constraints are active during the studies. Moreover, it is very important to select the objective function correctly in order to have a good behaviour in the algorithm solution.

Optimization is held mainly by a genetic algorithm (NSGA-II based) with 10 generations and a population size of 20, thus every procedure will run 200 designs.

Some test cases were run in order to analyse the proper objective functions to use (Study 1 in Section 6.1 for instance). Final studies look for a design that reduces the most the delivered power (eff_0) in comparison to an initial design (with delivered power P_{D0}). This is achieved essentially by reducing the torque and revolutions rate (see Equation 6.1).

$$eff_0 = 1 - \frac{2\pi Qn}{P_{D0}} \tag{6.1}$$

Another good objective would be the reduction of rudder forces. Rudder resistance reduction (R_{rudder}) could lead to a lower total ship resistance and in consequence reduce thrust and torque as well, resulting in a higher propulsion efficiency (η_D in Equation 2.15). However lateral force (Fy_{rudder}) is not taken into account due to uncertainties mentioned in Chapter 4.

As mentioned in Chapter 3.2, some variables are monitored to check the changes on the geometry, these are taken with respect to Y_{P1} (defined in Equation 3.1) at the chord with the highest twist at the top and bottom parts of the rudder, because it relates the input variables (angles and twist axis). These monitors are total twist of the geometry and rudder sweep, defined in Equation 6.2

$$Y_{total} = Y_{Top} - Y_{Bottom}, \qquad Y_{sweep} = \frac{Y_{Top} + Y_{Bottom}}{2} \tag{6.2}$$

6.1. Study 1: Sobol and NSGA-II based

This study was run in order to test the procedure and check the behaviour of algorithms if only one objective is selected, total resistance reduction for instance. A grid study was performed in order to double check the reliability of the coarse mesh with 16 $RefCells$ and discard errors due to mesh refinement. For this purpose, results were compared to a new study using a finer mesh with 22 $RefCells$.

In this study a first Sobol algorithm with 10 designs was run in order to define a semi random design space from an initial twisted rudder as reference ($Test000$). However, at this point no speed control for the operational point was used, thus results obtained with this algorithm are not comparable with the further NSGA-II based study, in which the speed control was used.

In order to select the "best" group of designs, first rudder longitudinal force is compared to Y_{sweep}. It is assumed that the best design area corresponds to zero sweep (or maximum total twist), this is when twist angles are equal but opposite.

In this study it was found that the fact that some designs have the lowest rudder longitudinal force, does not imply the lowest total resistance of the ship. This is because the rudder interacts with the propeller in a way such that the thrust can increase due to the rudders presence. On the other hand suction on the hull is increased as well, rising the hull resistance. This is why it was decided to look at the delivered power as an objective. This property is anyhow the most relevant when talking about propulsive efficiency. Some of the results thereby are presented in Table 6.1.

Table 6.1.: Study 1, NSGA-II based best designs

Design ID	Y_{sweep} [mm]	Y_{total} [mm]	P_D	eff_0	η_D
Non-twisted	-	-	43.6799	1	0.8044
Test000	-1.508	-15.621	43.4529	0.005196	0.8059
N-01-076	-0.1995	-9.5965	42.9579	**0.01653**	0.8146
N-01-111	0.0067	-9.5219	43.081	0.01371	0.8136
N-01-052	-2.6591	-7.9468	42.9482	0.01675	0.8143
N-00-223	-0.6043	-7.2328	43.3097	0.008474	0.8095
N-00-177	-0.6891	-11.887	42.9914	0.01576	0.8151

As shown, the optimization procedure is able to reduce the delivered power compared to an initial non twisted design (with bulb). An example is design N-01-076, with a reduction in delivered power eff_0 of 1.65% (or increase of 1% in propulsive efficiency η_D). This result is nonetheless not considered for the overall work, because the defined objective is minimization of total ship resistance in this specific case. Therefore a new study needs to be run with the correct objective function (delivered power) and subsequently the algorithm behaviour tends in the correct direction.

This study was used for a grid study comparing resistance both on rudder and ship, in order to confirm the reliability of the chosen mesh. In Figure 6.1 colors represent each force (or coefficient), with darker bars depicting chosen mesh Fine16 and lighter bars display results for mesh Fine22. Lateral force on the rudder ($Fy(rud)$) is included as well, just as monitoring value.

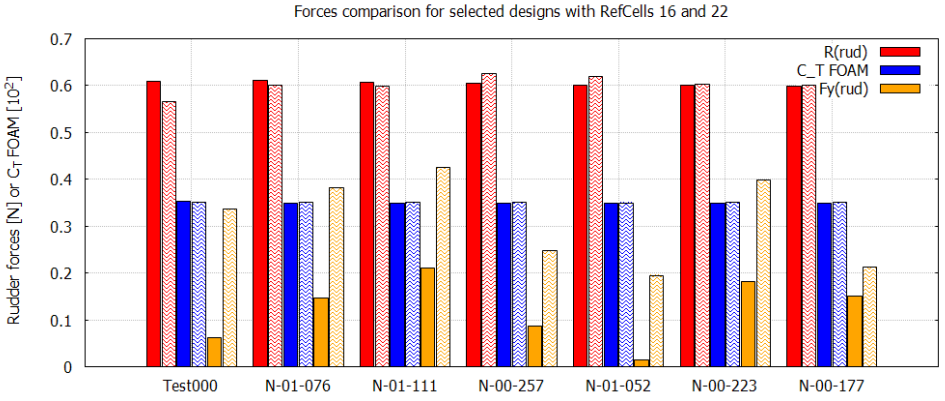

Figure 6.1.: Forces grid comparison for selected designs

It is exposed that the chosen mesh with $RefCells$ 16 is reliable for analysing total longitudinal forces, because it is not very sensitive to cell size in C_TFOAM (with delta lower than 0.5%). On the other hand, rudder resistance $R(rud)$ is still varying between 2% and 3%, which could not be accurate enough for an optimization work of such low order of magnitude. In any case, next studies present a new mesh study for designs considered as

optimal in order to double check the mesh. Moreover lateral force on the rudder is still presenting inconsistencies that need to be further studied in following researches.

6.2. Study 2: NSGA-II based

As mentioned in Study 1, a new optimization is run with a corrected objective. Another adjustment is applied to the design, twisting only the section included in the propeller slipstream. Having this new configuration, a NSGA-II based algorithm is run for 10 generations with a population of 20.

The adjustment on geometry in comparison with Study 1 is not huge but enough to influence the results. This design is the one presented in Chapter 3.2, which parametric function control points are in the area of influence of the propeller slipstream (see Figure 3.4).

In this case the objective is weighted for reduction in delivered power (in comparison to initial non-twisted rudder) and rudder resistance, in order to have a multi-objective optimization. The most important attribute to minimize is power with 80% weight, and remaining 20% to rudder resistance.

The design space is shown in Figure 6.2, in which the blue dotted line shows a so-called Pareto front. The Pareto front is mainly at negative Y_sweep, namely higher twist at rudders top side. A yellow design in the positive Y_sweep is detected and it might possess the lowest delivered power from the whole design space. Nonetheless it is far from the clustered designs and for this reason it is considered as a fluctuation or error in the overall calculations, therefore it is discarded.

Table 6.2 compiles the results for the 5 best designs (green in Figure 6.2) along with the design based on the SVA experimental test [11]. This design was run in a simulation because it is needed to have a numerical result to compare with a real twisted rudder.

From the table it is seen that the study converges in the expected range (negative Y_{sweep} close to zero), in which design N-200 presents the minimum delivered power, with a reduction with respect to the non-twisted rudder of 4.33% (or increase of 2.92% in propulsive efficiency). When comparing to the SVA test rudder, design N-200 has reduced the delivered power by 0.38%. Another good design is N-356, with a reduction in delivered power of 4.3% and increase in propulsive efficiency η_D of 2.93%.

This result shows that different designs can improve the efficiency in a similar way for the same propeller loading. In order to check which design could be better, a visual comparison is recommended. In this case it is shown in Figure 6.3 the differences in pressure coefficient between the two best designs N-200 and N-356 (non-twisted rudder as

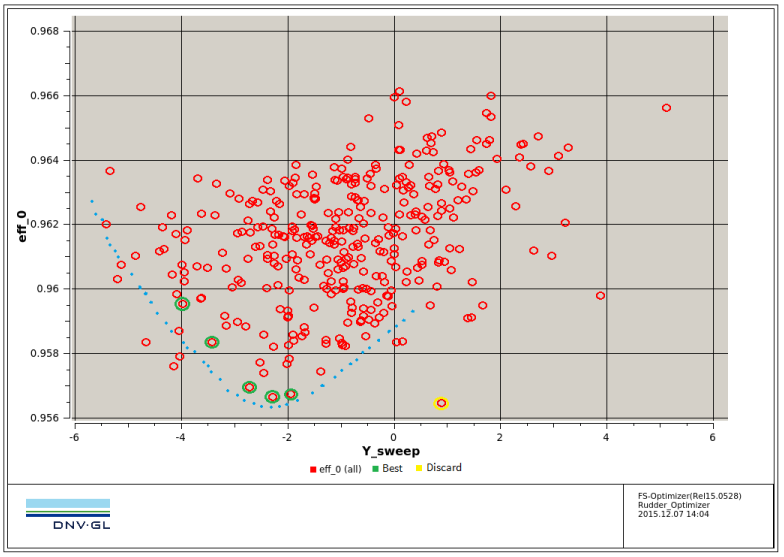

Figure 6.2.: eff_0 vs Y_{sweep}

Table 6.2.: Study 2, NSGA-II based best designs

Design ID	Y_{sweep}	Y_{total}	P_D	eff_0	η_D
Non-twisted	-	-	43.6799	0	0.8044
SVA-DTC	-0.2251	-6.0354	41.9462	0.0397	0.8326
N-188	-3.4281	-12.8458	41.8605	0.0417	0.8329
N-200	-2.2931	-8.2217	41.7866	**0.0433**	0.8336
N-314	-1.9568	-9.3588	41.7909	0.0432	0.8325
N-356	-2.733	-14.236	41.7996	0.043	**0.8337**
N-210	-3.9848	-13.5233	41.9127	0.0405	0.8325
N-256	-0.9258	-12.9552	41.8558	0.0418	0.8329

reference). It can be observed how the hub vortex is highly reduced by both designs, but mainly by N-356, which has a higher total twist.

Reducing the hub vortex (blue zone at the right of the bulb) and homogenizing the yellow zone surrounding the rudder can influence the rudder forces, because the pressure is homogenized. This helps to reduce the total resistance and, as a consequence, the power delivered by the propeller.

In Figure 6.4 the differences in axial velocity at the trailing edge are presented. It is observed that these velocities at both sides of the rudder tend to homogenize when twisting the leading edge, this is a consequence of minimizing the hub vortex. The circles highlight the most significant change with respect to the initial non-twisted design.

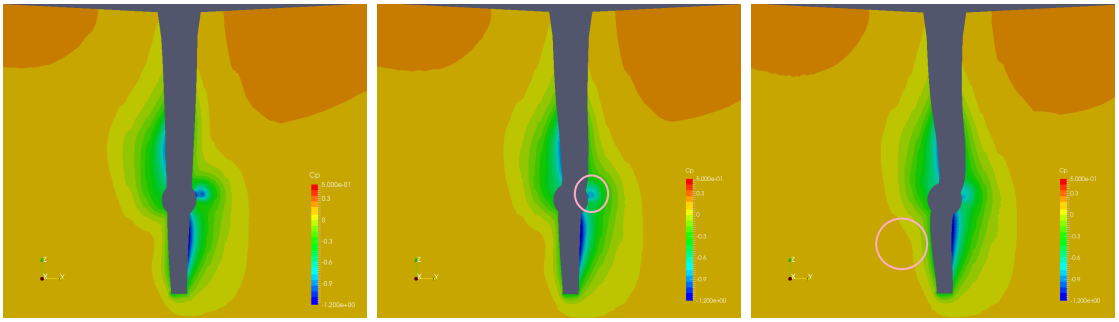

a) Non-twisted b) Design N-200 c) Design N-356

Figure 6.3.: Final Pressure coefficient contours at $X = 0.03$ (LE)

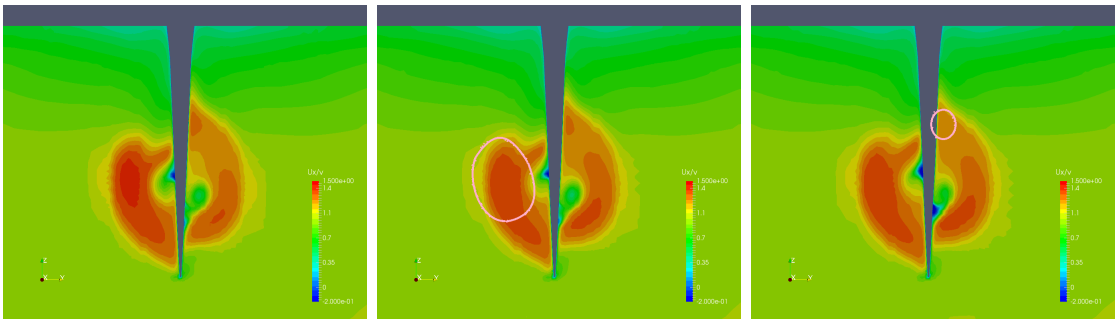

a) Non-twisted b) Design N-200 c) Design N-356

Figure 6.4.: Final Axial velocity contours at $X = -0.05$ (TE)

Finally, a comparison of the surface pressure is presented in Figure 6.5. The reduction of lateral pressure shown by design N-356 with respect to N-200 could cause a reduction on lift force by even half. This would mean that design N-356 is more suitable for manoeuvrability, because there would not be a need of correction for a zero angle incidence. This is however an assumption, because as aforementioned, this simulation is inadequate for measuring lateral forces until further mesh studies are approached. In the end both designs show how the optimization procedure could be accomplished using a coupled $RANS - BEM$ method. For further bulb studies, design N-200 is selected as reference.

6.3. Study 3: Bulb optimization

This study is a step further from the twist optimization, in which the variation of bulb parameters is analysed. As mentioned, bulb thickness, length and position are varied for the design selected in Study 2, N-200. The same algotithm NSGA-II based is used with 10 generations and a population size of 10. This study might be more sensible because of the very small order of magnitude in the results.

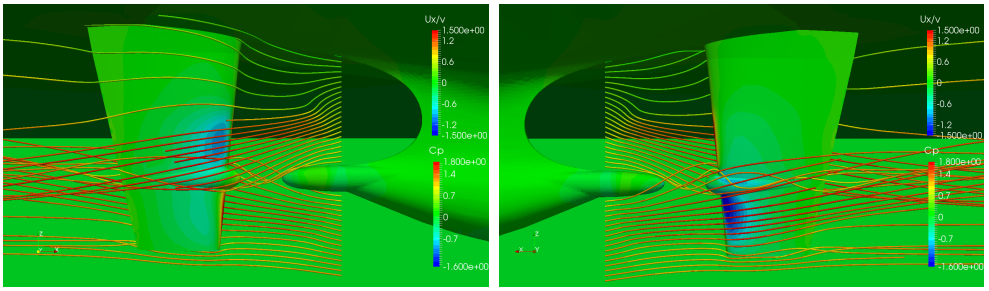

a) Design N-200 starboard b) Design N-200 port

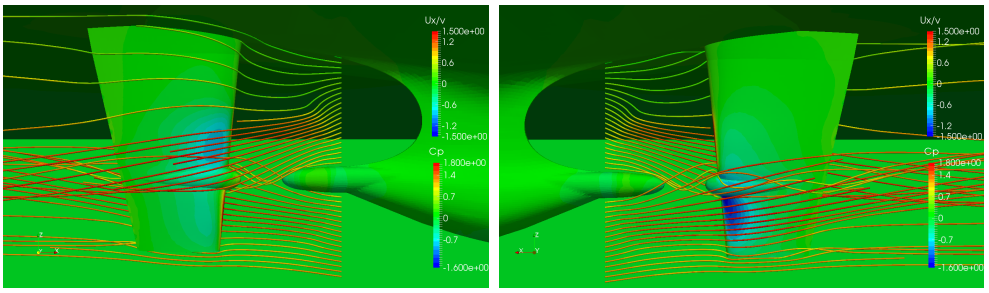

c) Design N-356 starboard d) Design N-356 port

Figure 6.5.: Streamlines view from Port and starboard (designs N-200 and N-356)

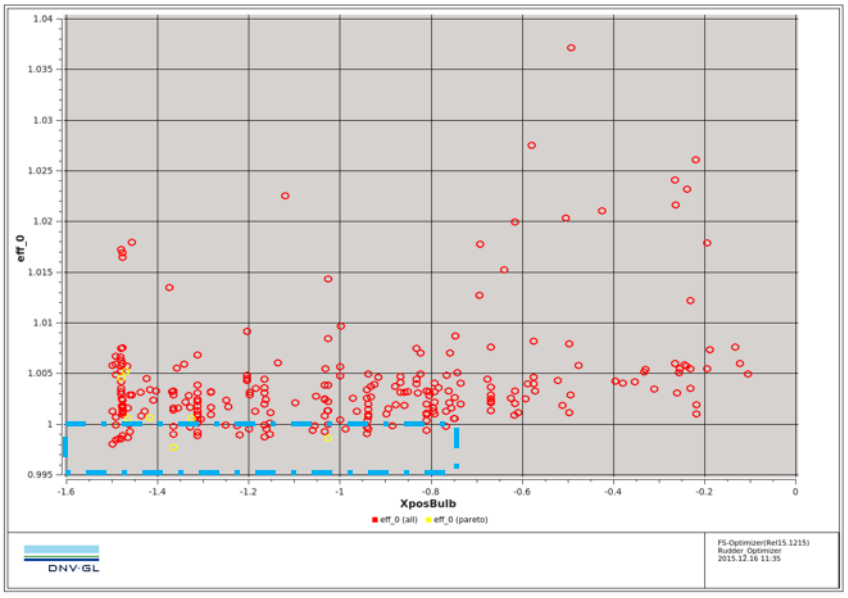

Figure 6.6.: DOE bulb optimization eff_0 vs X_pos

In Figure 6.6 the design space is shown, with the best designs highlighted. It is important to notice that in this case most of the designs are obtained for a eff_0 higher than 1. This means that results are showing an increase in delivered power compared to design N-200. The blue zone shows the valid results for our purpose. It is recommendable for future studies to use a constraint so eff_0 is always less than 1. Table 6.3 summarizes the data obtained for the three best designs observed.

Table 6.3.: Study 3, Bulb optimization best designs

Design ID	$ThicknessB$	$LengthB$	$XposB$	P_D	eff_0	η_D
N-200	0.2	6.5	0.1	41.7866	0.0433	0.8336
B-076	0.2323	8.9823	1.3668	41.6924	0.00225	0.8348
N-157	0.228	7.093	1.4995	41.7058	0.00193	0.8342
N-241	0.2462	6.7804	1.4923	41.721	0.00157	0.8333

As it can be observed, design B-076 presents a reduction in delivered power of 0.225% with respect to design N-200, increasing efficiency η_D by 0.12%. This means that changes on the bulb geometry do not affect the total ship efficiency in a great manner, but enough to reduce the propeller delivered power.

In figure 6.7 it is observed that compared to design N-200, in this case design B-076 has reduced almost completely the hub vortex due to the increase in bulb size. The axial velocity at the TE is basically not changed, it only has a more defined shape (more circular and closer to the rudder), which could mean an alignment of the flow with the bulb length.

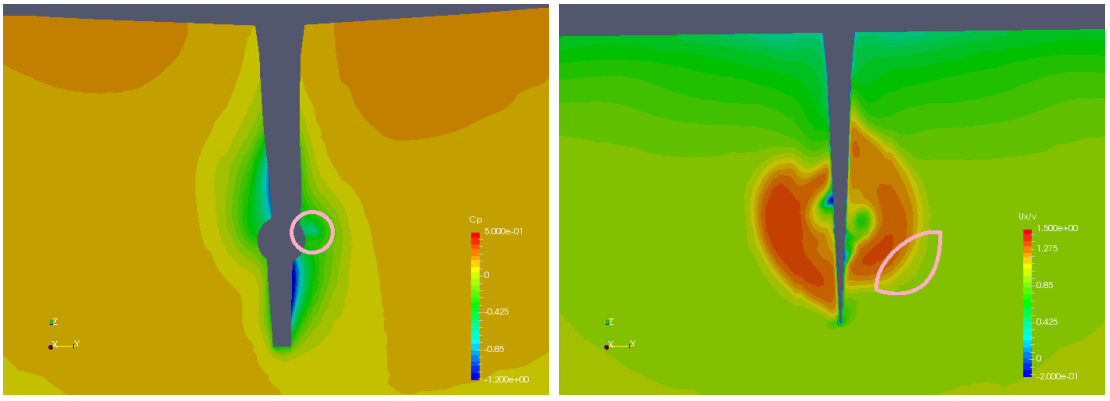

a) Pressure coefficient at LE b) Axial velocity at TE

Figure 6.7.: Final Pressure coefficient and axial velocity contours design B-076

Finally in Figure 6.8 the difference in pressure distribution over the rudder is appreciated. The hub vortex pressure on the bulb is almost imperceptible and the streamlines look more aligned to the bulb specially because of the reduction in the distance between Hub and bulb. This gives us a trace on how an optimum bulb design should look like: longer than rudder and as close to the hub as possible. Even if these results are not affecting the total ship propulsive efficiency, the behaviour of the flow surrounding the rudder would determine some manoeuvre conditions and delivered power. This topic is recommended to study in detail in further researches.

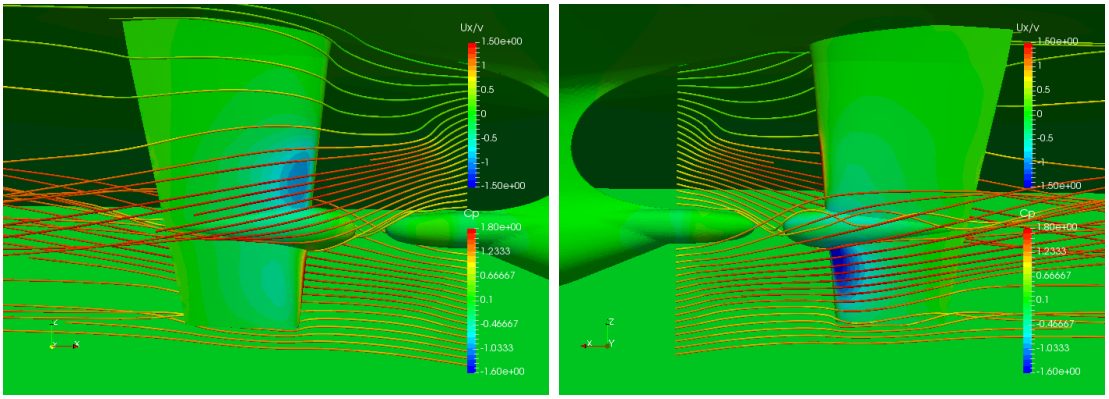

a) Starboard b) Port

Figure 6.8.: Streamlines view from Port and starboard design B-076

6.4. Final Grid study

A final grid study was performed to the 6 best designs selected from Study 2 and 3, with the purpose of a final check to the mesh refinement accuracy. The same methodology as presented in Study 1 is used, with darker bars corresponding to mesh Fine16 and lighter bars to Fine22. In this case convergence of total resistance coefficient (C_TFOAM), propulsion efficiency and rudder resistance ($R(rud)$) are shown in Figure 6.9.

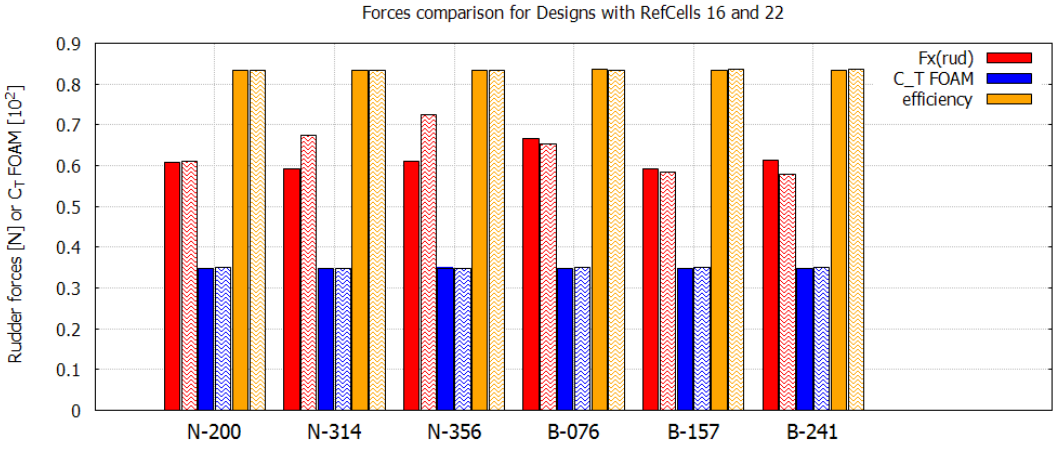

Figure 6.9.: Forces grid comparison for best designs

It is clear that there are still some inconsistencies on the rudder forces, with differences up to 13% which is not acceptable in the frame of this work. However, for total ship results as resistance or propulsion efficiency, mesh Fine16 is accurate enough with differences lower than 1% compared to Fine22. This means that for the optimization of the propulsive efficiency, the results can be regarded as valid, but if it is necessary to study the rudder itself, the mesh quality is not high enough and further research is recommended.

7. Conclusions

The main objective of the present work was the assessment of an optimization methodology for propulsion efficiency using a twisted rudder with costa bulb. This method is implemented utilizing a coupled RANS-BEM method and in-house software.

The coupled *RANS-BEM* method is used to have an interface for solving such a complex fluid dynamics problem (Hull-Propeller-Rudder interaction) by means of two theories: Potential Flow for propeller and stationary Reynolds Averaged Navier-Stokes equations for hull and rudder. This method is capable of solving the problem in a considerably reduced computational time compared to a full RANS approach. For instance, using a refined mesh the solution takes between 5 and 8 [1] hours for one rudder design, while a RANS study could take about 2 to 3 days.

Mesh refinement takes a very high level of importance when optimizing a rudder, since the differences between one design to another are very small (in terms of resistance and thrust), thus the admissible error of the solution on a final (refined) mesh must be smaller than the optimization level. In this case, mesh convergence is based on a 2% criterion, in order to achieve an optimization higher than this error.

When using an optimization method, the most important parameters to take into account are: variable selection, optimization algorithm and choice of objectives. A clever selection and definition of the variables also determine the possible geometry variations. The combination of them can significantly reduce the required computational effort, therefore variable selection is crucial for an efficient and effective optimization. A correct algorithm defines the design space and computational time to find the so called Pareto front with optimum designs. Objective definition grants the path to an appropriate solution.

In this work variables are selected from rudder and bulb geometric parameters (twist angle and axis, bulb thickness, length and position). The algorithm is based on a NSGA-II, included in the in-house FS-Optimizer. Objectives are selected for different studies based on resistance reduction or delivered power reduction. The last one presents a better performance in optimizing the propulsion efficiency when modifying the rudder twist and bulb.

The solution of a NSGA-II based design of experiments (about 200 designs in each study presented in this work) takes around 4 to 5 days in computational time. This, compared

[1] with 24 cores on a cluster node with 2.4GHz AMD Opteron 6234 Cpu's

to a gradient method is significantly faster. For instance, a T-search method was tested, taking almost the same time for solving only 40 designs and yet without finding the optimum twisted rudder. At this stage the starting point for T-search is of high importance because of its nature as deterministic method, such that it can actually find the same minimum as the stochastic NSGA-II. This comparison is difficult in any case, due to the different natures of the algorithms.

The optimization method was run initially for getting the best twist angle possible for the propeller load, here two designs are selected as best: N-200 and N-356 with a reduction in delivered power of 4.33% and 4.3% respectively. Based on design N-200 a new optimization run was held changing only the bulb parameters.

The last run, corresponding to the bulb optimization shows an extra reduction of delivered power of 0.225%, showing that bulb parameters do not affect the propulsion efficiency in the same amount as the rudder twist. However, a good bulb design improves the flow alignment around the rudder. The results of the optimization indicate that the bulb should be longer than the rudder and close to the propeller hub to reduce the gap which induces a high swirl in front of the rudder.

As shown, the method is capable of small scale optimization as in the case of a twisted rudder, but as mentioned, some characteristics are decisive to find the appropriate solution path for the algorithm. The next chapter outlines a number of recommendations for the improvement of the results in further studies

8. Recommendations

The coupled method developed by Schenke [14] does not include an overall convergence criterion, therefore it is recommendable to implement such methodology to find an optimum solution at a minimal number of iterations. This could help to reduce the computational time.

As mentioned in Chapter 2.2, an error is induced when assuming the free surface resistance from an initial design but not calculated for every new design. Although it is assumed that this error barely affects the final optimization results, it is recommendable to run a further study to investigate the validity of this assumption.

Another suggestion is an improvement of the parametric model, in order to have access to all geometric properties by means of parametric functions. Thus the optimization methodology could control all desirable variables.

The last bulb optimization study was performed only for design N-200. The algorithm could find a better solution if all variables are controlled simultaneously, this is: rudder and bulb properties. This way the optimization procedure is able to find the best design possible both for bulb and rudder at the same time. This will increase the design space drastically as more generations are required.

During the development of this master thesis, it is mentioned that the procedure is not able to achieve an accurate calculation of the rudder forces. It is advisable to deeply study this situation by modifying mesh refinement or simulation parameters.

For better analysis of a best chosen design, further simulations should be carried out. New conditions could be studied, such as different propeller loads, rudder angle and drift angle.

Finally, with a deep study of the ideal rudder design, it is important to perform a towing tank test to validate the results obtained in every condition.

9. References

[1] B. Andersson, R. Andersson, L. Håkansson, M. Mortensen, R. Sudiyo, and B. Van Wachem. *Computational Fluid Dynamics for Engineers*. Cambridge University Press, 2011.

[2] I. J. Bosschers. *PROCAL v2.0 THEORY MANUAL*. MARIN, June 2009. 2 Haagsteeg, P.O. Box 28 6700 AA Wageningen, the Netherlands.

[3] D. Cappelli and N. N. Mansour. Performance of reynolds averaged navier-stokes models in predicting separated flows: Study of the hump flow model problem. In *44th AIAA Thermophysics Conference*, 19-21 Dec 2012.

[4] K. Deb. A fast and elitist multiobjective genetic algorithm: Nsga-ii. *IEEE TRANSACTIONS ON EVOLUTIONARY COMPUTATION*, 6(2), 2002.

[5] DNV-GL. *FS-Optimizer User manual*. FutureShip, February 2014.

[6] J. Herbel. Development of a robust automated meshing process for the simulation of propeller-rudder-hull interaction using star-ccm+ and openfoam. Master's thesis, Hochschule Bremen, 2014.

[7] K. Hochkirch and V. Bertram. Options for fuel saving for ships. Technical report, FutureShip GmbH, 2009.

[8] ICCT. *The Energy Efficiency Design Index (EEDI) for New Ships. www.theicct.com*, 2011.

[9] J. Katz and A. Plotkin. *Low-Speed Aerodynamics: From Wing Theory to Panel Methods*. McGraw-Hill Book Co, 1991.

[10] A. Molland F. and S. R. Turnock. *Marine Rudders and Control Surfaces. Principles, data, design and applications*. Elsevier Ltd, 2007.

[11] T. Nietzschmann. Widerstands- und Propulsionsversuch für das Modell eines Containerschiffes, Modell M1398S001, Propeller P1570. Technical report, Schiffbau-Versuchsanstalt Potsdam, Marquardter Chaussee 100, 14469 Potsdam, Germany, December 2010.

[12] H. Nilsson and W. Gyllenram. Experiences with openfoam for water turbine applications. In *Proceedings of the 1st OpenFOAM International Conference*.

[13] A. Sarasquete F. and A. Caldas C. Investigación sobre la eficiencia energética en timones. Technical report, Líneas de investigación en Vicus Desarrollos Tecnológicos S.L., 2009.

[14] S. Schenke. Assessment of propulsion efficiency for hull-propeller systems. Master's thesis, TUHH, 2015.

[15] S. Schenke. *RANS-BEM-Coupling Using PROCAL and OpenFOAM*. DNV-GL, September 2015.

[16] E. C. Tupper. *Introduction to Naval Arquitecture*, chapter 8. Propulsion. Elsevier Ltd., 2004.

[17] S. Turnock and A. Molland. Energy efficieny of ship propulsive systems: rudder-propeller interaction. In *Ship Propulsion Systems Conference*, page 30. London: Institute of Marine Engineering Science and Technology, 2010.